NASA TECHNICAL NOTE

NASA TN D-3973

NASA TN D-3973

STUDY OF DYNAMIC RESPONSE TO IMPACT LOADINGS OF ACCELERATION SENSORS HAVING VARIOUS MOUNTING CHARACTERISTICS

by John Locke McCarty and Jerome Pearson

Langley Research Center

Langley Station, Hampton, Va.

NATIONAL AERONAUTICS AND SPACE ADMINISTRATION • WASHINGTON, D. C. • MAY 1967

NASA TN D-3973

STUDY OF DYNAMIC RESPONSE TO IMPACT LOADINGS OF ACCELERATION SENSORS HAVING VARIOUS MOUNTING CHARACTERISTICS

By John Locke McCarty and Jerome Pearson

Langley Research Center
Langley Station, Hampton, Va.

NATIONAL AERONAUTICS AND SPACE ADMINISTRATION

For sale by the Clearinghouse for Federal Scientific and Technical Information
Springfield, Virginia 22151 – CFSTI price $3.00

STUDY OF DYNAMIC RESPONSE TO IMPACT LOADINGS OF ACCELERATION SENSORS HAVING VARIOUS MOUNTING CHARACTERISTICS

By John Locke McCarty and Jerome Pearson
Langley Research Center

SUMMARY

An analytical investigation was performed to study the dynamic response to impact loadings of acceleration sensors having various mounting characteristics. Analytically represented impacting bodies were subjected to input force pulses of half-sine, triangular, quarter-sine, and rectangular shapes, approximating typical target impact acceleration signatures. Studies were made with an analog computer of the acceleration time histories measured by acceleration sensors of different mass which are coupled to the impacting body by a mounting system having various combinations of damping and spring stiffness.

Boundaries for the system parameters were established that defined conditions for which the accelerometer assembly and its coupling have a negligible effect on the accelerations experienced by the impacting body. These boundaries define ranges of the parameters of the two-degree-of-freedom system for which the impact response characteristics can be evaluated from a single-degree-of-freedom analysis. Further, with a knowledge of these parameters and the impact velocity, the shape and the magnitude of specific input pulses applied to the impacting body can be defined from characteristics of the acceleration-time-history response of an acceleration sensor mounted to that body.

INTRODUCTION

The Langley Research Center has been actively engaged for several years in developing a dynamic penetrometer technique as a means for determining physical properties of a remote surface such as that of the moon or planets (refs. 1 to 3). This technique consists of impacting the surface in question with accelerometer-equipped projectiles called penetrometers and analyzing the accelerations generated during the impact process. The results of penetrometer impact studies conducted on a variety of target surfaces (refs. 4 and 5) have shown that this technique is amenable to defining certain physical properties of the impacted material.

Penetrometers are designed such that all accelerations of the impacting body are experienced by the acceleration sensor; however, variations to the penetrometer technique are being considered wherein acceleration sensors would be integrated with other devices in multimission payloads designed to impact the moon or planets. The purpose of the sensor in these applications would be to provide those payloads with a surface-measuring capability. The output of the sensor in such combined payloads would not necessarily reflect the accelerations of the impacting body since these accelerations are transmitted to the sensor through a flexible structure which could mask significant details of the body accelerations. Furthermore, the presence of a flexibly mounted accelerometer assembly can influence the accelerations experienced by the impacting body. If the impact data collected from acceleration sensors are to be meaningful in evaluating surfaces, they must be interpreted in terms of the forces applied by the target material to the impacting body. The objective of this paper is twofold: to determine the conditions for which the accelerometer coupling in a combined penetrometer-type payload influences the accelerations experienced by the impacting body and to evaluate the effect of the accelerometer coupling on pertinent characteristics of the acceleration time histories sensed by the accelerometer during impact.

Data are available which treat the transient response of single-degree-of-freedom systems to various forcing functions. References 6 to 9, for example, consider the response of an undamped system to several input pulse shapes, and reference 10 includes the effect of damping on the response of accelerometers to several transient acceleration pulses over a narrow range of pulse frequencies. These studies are limited to the analysis of a one-degree-of-freedom system; however, for penetrometer secondary payload applications, a two-degree-of-freedom analysis is necessary to define the response of the system because the effect of the accelerometer and its mount on the motions of the impacting body must be included. Further, the reference studies consider only the peak acceleration response to input transients which is but one of the response characteristics considered necessary to define adequately the acceleration time history of the impacting body.

This report discusses the results of an analytical investigation undertaken to study the dynamic response to impact loadings of acceleration sensors having various mounting characteristics. In the investigation, conducted on an analog computer, bodies were subjected to input force pulses of half-sine, triangular, quarter-sine, and rectangular shapes, approximating typical target impact acceleration signatures, and studies were made of the acceleration time histories measured by acceleration sensors of different mass which are coupled to the impacting body by a mounting system of variable characteristics.

SYMBOLS

a	peak acceleration of accelerometer assembly
c	damping coefficient
$F(t)$	input force (forcing function)
F_{max}	maximum value of input force
k	stiffness of coupling between accelerometer assembly and impacting body
m	total system mass, $m_1 + m_2$
m_1	mass of impacting body
m_2	mass of accelerometer assembly
t	time
t_R	rise time for peak acceleration in input acceleration time history
t_T	total pulse time for input acceleration time history
t_r	rise time for peak acceleration in accelerometer assembly acceleration time history
t_t	total pulse time for accelerometer assembly acceleration time history
x_1	displacement of impacting body
x_2	displacement of accelerometer assembly
α	peak acceleration of input, F_{max}/m
ζ	fraction of critical damping, $\frac{c}{2\sqrt{km_2}}$
ω	frequency associated with input acceleration time history, π/t_T

ω_n undamped natural frequency of accelerometer assembly, $\sqrt{k/m_2}$

ω' frequency associated with accelerometer assembly acceleration time history, π/t_t

Dots over symbols represent time derivatives.

ANALYSIS

Description of System

The analysis treated a typical penetrometer represented schematically as the two-degree-of-freedom system shown in figure 1. This system consists of the impacting body of mass m_1, the accelerometer assembly of mass m_2, and the accelerometer mount represented by the spring constant k and the damping coefficient c. The force applied to the impacting body by the target is represented by the time history $F(t)$. The displacements of the impacting body and the accelerometer assembly are denoted by x_1 and x_2, respectively, which are measured from an arbitrary reference.

Equations of Motion

The equations of motion for the masses m_1 and m_2 of figure 1 are

$$\left.\begin{aligned} m_1\ddot{x}_1 - k(x_2 - x_1) - c(\dot{x}_2 - \dot{x}_1) - F(t) = 0 \\ m_2\ddot{x}_2 + k(x_2 - x_1) + c(\dot{x}_2 - \dot{x}_1) = 0 \end{aligned}\right\} \tag{1}$$

For convenience, the natural frequency ω_n and damping ratio ζ of the accelerometer assembly are defined for the condition in which m_1 is clamped. For this condition $\omega_n = \sqrt{\frac{k}{m_2}}$ and $\zeta = \frac{c}{2\sqrt{km_2}}$. With these relationships the equations of motion can be written in the form

$$\left.\begin{aligned} \ddot{x}_1 - \frac{m_2}{m_1}\omega_n^2(x_2 - x_1) - \frac{m_2}{m_1}2\zeta\omega_n(\dot{x}_2 - \dot{x}_1) - \frac{1}{m_1}F(t) = 0 \\ \ddot{x}_2 + \omega_n^2(x_2 - x_1) + 2\zeta\omega_n(\dot{x}_2 - \dot{x}_1) = 0 \end{aligned}\right\} \tag{2}$$

These equations were solved with the aid of an analog computer.

Ranges of Parameters

The computer solutions to equations (2) describe the response of the system to various impact force time histories over a range of nondimensional system parameters. Impact force time histories F(t) were represented by half-sine, triangular, quarter-sine, and rectangular pulse shapes as illustrated by the acceleration time histories of figure 2. These pulse shapes, which are easily described and mathematically defined, approximate the response of penetrometers impacting onto various classes of target materials (ref. 4). The half-sine and triangular pulse shapes approximate elastic impact conditions normally characterized by a pulse which is symmetrical about a mean vertical line passing through the peak acceleration. The quarter-sine pulse corresponds to a plastic collision described by an acceleration time history with a brief restitution increment. This shape also approximates the penetrometer accelerations during the crushing of most shock absorbing materials used in impact limiters. The rectangular pulse shape typifies the response of a projectile impacting onto a target material which offers constant resistance with penetration (collapsible failure mode). The duration of each pulse is the time t_T, and the associated frequency ω is defined as $\omega = \pi/t_T$.

System parameters included the frequency ratio, defined as the ratio of the accelerometer assembly undamped natural frequency to the frequency of the input force, ω_n/ω; the mass ratio, defined as the ratio of the impacting body mass to the mass of the accelerometer assembly, m_1/m_2; and the damping ratio of the accelerometer assembly ζ. Solutions to the equations were obtained for each input pulse shape over the following ranges of system parameters of current practical interest: frequency ratio from 0.1 to 50, mass ratio from 0.2 to 100, and damping ratio from 0.01 to 0.10.

RESULTS AND DISCUSSION

To be of value in describing the target material, the acceleration response data of an impacting penetrometer-type device must be interpreted in terms of the forces applied by the target to the impacting body. Hence, the acceleration time history of the impacting body must closely approximate the acceleration time history of the input; that is, the impacting body must be negligibly affected by an accelerometer or other flexibly mounted component. In a two-degree-of-freedom system there generally is interaction between the motions of the two masses – the acceleration of one affecting that of the other. However, there exist certain combinations of system parameters for which the effect of one mass on the other is negligible. In the present system there are certain values of the mass, frequency, and damping ratios for which the effect of the accelerometer assembly on the motion of the impacting body is not negligible. For these conditions, the impacting body acceleration time history no longer duplicates that of the input force.

Figure 3 presents reproductions of analog computer solutions to illustrate how variations in system parameters influence the response of the two masses. Figure 3(a) shows the effect of changes in the frequency ratio on the response to a half-sine forcing function for a system having a mass ratio of 5 and figure 3(b) shows the effects for a system having a mass ratio of 100. In this figure, the acceleration scales for the input and for the responses of the two masses, m_1 and m_2, are the same for both mass ratios and for all frequency ratios. For a completely rigid system, corresponding to a frequency ratio of infinity, the time histories of acceleration for the input $F(t)/m$, for the impacting body $\ddot{x}_1$, and for the accelerometer assembly $\ddot{x}_2$ would be identical, regardless of the mass ratio. However, the figure shows that as the coupling between the two masses becomes more flexible, corresponding to lower frequency ratios, the response of the accelerometer assembly differs markedly from the input accelerations. At a frequency ratio of 50 which corresponds to a system employing a stiff coupling, there is a slight evidence of the high accelerometer assembly frequency superimposed upon the response of $\ddot{x}_2$ to the input force, whereas at the somewhat lower frequency ratios of 3 and 1, the magnitude and shape of $\ddot{x}_2$ have deviated appreciably from the input accelerations.

The influence of the coupled accelerometer force is dependent not only upon the frequency ratio as illustrated in figure 3(a) but also upon other parameters of the system such as the amount of damping and, as shown in figure 3(b), the system mass ratio. For the high frequency ratio, $\ddot{x}_1$ reproduces the input force time history with no apparent contribution from the high frequency motions of $\ddot{x}_2$; however, at low frequency ratios the impacting body accelerations are considerably affected by the accelerometer assembly forces at a mass ratio of 5 (fig. 3(a)). At a mass ratio of 100 (fig. 3(b)) there is no apparent effect of $\ddot{x}_2$ on $\ddot{x}_1$ since the latter closely duplicates the input.

In figures 3(a) and 3(b) the input force applied to m_1 is the same for both mass ratios. Furthermore, the magnitude of the accelerations of m_2 is similar for both cases. However, there is a noticeable difference in the response of m_1 which is attributed to differences in the magnitude of the forces associated with the accelerations of m_2. For the same acceleration, the force exerted by the accelerometer assembly on the impacting body decreases with increasing mass ratio since the system total mass is constant. It is apparent from figure 3 that for certain combinations of the system parameters the response of $\ddot{x}_1$ closely duplicates the input force time history. It is for these conditions ($\ddot{x}_1$ unaffected by the motions of m_2) that the input force time history can still be inferred from the time history of $\ddot{x}_2$ even though $\ddot{x}_2$ may be different from $\ddot{x}_1$.

Criteria for Acceptability

In order to establish what combinations of system parameters produce acceptably small effects of the accelerometer assembly on the motion of the impacting body, it was necessary to select suitable criteria for acceptability. Permissible deviations in the acceleration of the impacting body were selected consistent with the accuracy of present-day shock measuring and recording systems. More specifically, to be considered satisfactory, the impacting body accelerations were required to reproduce the accelerations due to the input force to within ±10 percent of the peak value, α, as shown in figure 4. (The peak value of acceleration due to the input force is defined as $\alpha = F_{max}/m$ where F_{max} is the maximum value of the input force and $m = m_1 + m_2$.) If the impacting body accelerations reproduce the input accelerations to within ±5 percent α throughout the duration of the input force, the effect of the accelerometer and mount on the motion of the impacting body was considered tolerable and the input accelerations were assumed to have been acceptably reproduced. Time histories having deviations between ±5 and ±10 percent α were treated as marginal reproductions of the input accelerations, and those having deviations exceeding ±10 percent α were considered unacceptable reproductions. In addition to that applied to amplitude, restrictions were also placed upon characteristic times of the impacting body acceleration time history. Both the total pulse time and the time to peak amplitude were required to be within ±5 percent of the corresponding times of the input acceleration to be acceptable. If the amplitude and characteristic times of the impacting body acceleration time history were found to be acceptable or marginal based upon these criteria, the input accelerations were considered to have been satisfactorily reproduced, and the response of the accelerometer assembly could then be analyzed. With the use of these criteria, each parametric condition was examined for acceptable, marginal, or unacceptable impacting body accelerations. Figure 5 presents sample analog computer solutions to illustrate the application of the criteria for acceptability to the impacting body acceleration time histories. For a given pulse shape, boundaries based upon the system parameters were faired through the marginal cases, separating acceptable from unacceptable conditions.

Boundaries for Application

The boundaries for application which define the system parameters whereby the accelerations of the impacting body reproduce the input accelerations according to the criteria for acceptability are given in figure 6. These boundaries are presented as functions of frequency ratio and mass ratio for different pulse shapes and damping ratios. Only those data necessary to define the boundaries are included in the figure. Figures 6(a) and 6(b) show that, for the half-sine and triangular pulses, as the mass ratio is increased the input accelerations are satisfactorily reproduced at decreasing frequency

ratios. The boundary for the rectangular pulse (fig. 6(d)) is independent of frequency ratio and the amount of damping and is a function of only the mass ratio. The instantaneous acceleration ($t_R = 0$) of this input pulse introduces oscillations in the impacting body response, $\ddot{x}_1$, greater than ±10 percent α for mass ratios 10 and below. (See fig. 5.) The impacting body response for these mass ratios does not fulfill the amplitude criteria for acceptability.

Similar impacting body response occurs for the quarter-sine input pulse (fig. 6(c)) due to the instantaneous decrease in acceleration at the pulse terminator. For this pulse, the oscillations in $\ddot{x}_1$ occur beyond the conclusion of the input pulse. (See fig. 5.) At test mass ratios greater than 10, this oscillation is less than ±10 percent α and the accelerometer response can be analyzed to describe the target input. For lower mass ratios, the oscillation in $\ddot{x}_1$ following the input pulse terminator exceeds ±10 percent α. However, for certain frequency ratios, the peak accelerometer response occurs prior to this oscillation, and the peak acceleration a and corresponding time t_r of the accelerometer offer meaningful data since up to that time the impacting body response duplicates the input. This additional boundary is also included in figure 6(c).

The effect of damping on the boundaries for application is best illustrated with the aid of figure 7 which summarizes the boundaries faired for the half-sine pulse over a range of damping ratio between 0.01 and 0.10. This figure shows that, for this pulse shape, the region of acceptable data is enlarged with increased damping. A comparison of all data of figure 6 shows that this trend is the same for all examined pulse shapes that do not involve instantaneous changes in accelerations or decelerations. The immediate response to pulse shapes having step changes in accelerations or decelerations is the same for all examined damping ratios; however, as expected, the oscillation in the response following such an abrupt acceleration change decays much more rapidly with increased damping.

Acceleration Time Histories

Acceleration time histories recorded during the impact of penetrometers or accelerometer-equipped projectiles on target surfaces exhibit characteristics which are of significance in defining the impacted surface. These characteristics are noted in the sample accelerometer response of figure 2(e) and include the magnitude of the peak acceleration a, the rise time required to reach that acceleration t_r, the total duration of the pulse t_t, and the overall shape of the acceleration time history. Figure 8 presents typical responses of the accelerometer assembly to the input force pulses for specific frequency ratios. In this figure, the acceleration of the accelerometer assembly $\ddot{x}_2$ is nondimensionalized with respect to the maximum input acceleration α and time is related to the duration of the input force, t_T. (See fig. 2.) Characteristics of these

and all other acceleration time histories are presented in figures 9 to 15 in terms of the corresponding characteristics of the input force. These characteristics as affected by the system parameters and the shape of the input force pulse are discussed in the following sections.

Peak acceleration.- The acceleration time histories of figure 8 show distinct differences in the magnitude of the peak acceleration with variations in the frequency ratio. These differences are better illustrated in figure 9 where the ratio of peak acceleration measured by the accelerometer to the peak input acceleration a/α is plotted as a function of the frequency ratio for two damping values. Data are presented for all mass ratios evaluated and found from the assumed criteria to be either acceptable or marginal. The curves of this figure were faired through the data obtained from the highest evaluated mass ratio, $m_1/m_2 = 100$; however, in general, these curves agree with the data for all mass ratios, particularly for the higher ratio of damping.

Figure 9 shows that at low frequency ratios, corresponding to weak accelerometer mounts (low values of k), the acceleration levels sensed by the accelerometer are considerably less than those of the input force. These peak accelerations increase with increasing frequency ratio to a value which exceeds that of the input force, reaching a maximum at frequency ratios less than 2. Except for the response to the rectangular pulse, the peak accelerations decrease with any further increase in the frequency ratio in a decaying oscillation about an acceleration level which converges upon the input peak acceleration. For the rectangular input force (fig. 9(d)), the peak acceleration reaches a maximum value at a frequency ratio of unity and remains at that value for all higher frequency ratios. In other words, above a frequency ratio of unity, the maximum response to a rectangular pulse is independent of the duration of the pulse and is the same as though the input force were not removed.

The effect of damping on the magnitude of the accelerometer peak accelerations is shown for each input pulse shape in figure 9 for damping ratios of 0.01 and 0.10. The effect is better illustrated in figure 10 where the peak acceleration data for the half-sine input pulse is combined with that for two additional intermediate values of damping for a mass ratio of 100. These curves show that with increased damping, the peak accelerations are decreased and that the frequency ratio at which peak acceleration reaches a maximum is independent of the damping. Furthermore, since increased damping reduces the acceleration level, for all pulse shapes except the rectangular shape, the higher the damping the lower is the frequency ratio at which the peak acceleration level converges on that of the input. Therefore, on the basis of peak acceleration alone, for these pulse shapes, the higher the damping the narrower is the range of frequency ratios where the accelerometer does not reproduce the input.

Figure 11 is a composite of peak acceleration data for all pulse shapes. The figure also presents the results of a single-degree-of-freedom analysis (ref. 6) available for the half-sine, triangular, and rectangular pulse shapes. The reference data are based upon an undamped system having an infinite mass ratio and is seen to be closely duplicated by the present system with a mass ratio of 100 and a damping ratio of 0.01. These data are also supported by the analytical results of references 7 to 10. Since the magnitude of the peak accelerations decreases with increasing damping, the acceleration levels of figure 11 for an undamped system constitute the maximum obtainable values. According to this figure and the text of reference 6, the maximum values are 2.00 for the rectangular pulse, 1.75 for the half-sine pulse, and 1.52 for the triangular pulse. The quarter-sine pulse, not noted in this reference, has a maximum peak acceleration ratio of about 1.53 as obtained from the present calculations. Reference 6 explains that the maximum peak acceleration associated with the rectangular pulse is greater than that of the other pulses because the latter have finite rise times.

Figure 11 illustrates trends which are of significant interest to the interpreter of penetrometer-type impact data. At low frequency ratios (less than about 5) where the peak accelerations of the sensor differ markedly from those of the input force, there exist differences in the peak acceleration levels of the various input pulse shapes. These differences, which also exist with damping, appear sufficient to permit a definition of the forcing function. At higher frequency ratios the differences in the peak acceleration levels are not as pronounced and the forcing function is not easily determined from peak acceleration information alone. However, these levels of acceleration approach that of the input force, particularly with the presence of damping which expedites the convergence, and the different input pulse shapes become more recognizable from the acceleration time history of the accelerometer as shown by the data of figure 8 at high frequency ratios.

Characteristic times.- The accelerometer responses of figure 8 reveal that with variations in the frequency ratio, differences not only exist in the magnitude of the peak acceleration but also in the characteristic times of the acceleration time histories. These differences are exemplified for all conditions in figures 12 and 13 where the characteristics rise time t_r and total pulse time t_t divided by the corresponding characteristic times of the input acceleration time histories t_R and t_T, respectively, are presented as a function of the frequency ratio for two damping values. The nondimensional rise times for each pulse shape are presented in figure 12 and the nondimensional total times are presented in figure 13. Again, data are presented for all mass ratios found from the criteria to be acceptable or marginal. In these figures, the data from the highest mass ratio, $m_1/m_2 = 100$, were faired by curves which, in general, describe the data for all mass ratios. Characteristic times measured from data of references 6 and 10 for undamped

single-degree-of-freedom systems are also included in the figures for the half-sine, triangular, and rectangular input pulse shapes where $\zeta = 0.01$ for purposes of comparison.

Figure 12 shows that the rise times associated with the accelerometer response are a maximum at the lowest frequency ratio of this investigation, 0.1, and become equal to those of the input at frequency ratios between 20 and 50. The response rise time to the half-sine pulse (fig. 12(a)) decreases from a value approximately 10 times that of the input at $\omega_n/\omega = 0.1$ to a value somewhat less than that of the input $(0.6t_R$ to $0.7t_R)$ at a frequency ratio of about 5. At this frequency ratio the accelerometer response rise time shifts to a duration longer than that of the input as a result of the oscillations in the accelerometer response time history. (See figs. 2(e) and 8(a).) The relationship between the rise time of the response and that of the input appears to be undulatory in nature at frequency ratios between 5 and 20. The rise time of the accelerometer response to the triangular pulse (fig. 12(b)) differs from that of the half-sine only in that it appears never to become less than the rise time of the input but, instead, approaches the input time in an asymptotic manner. The rise time of the response to the quarter-sine pulse (fig. 12(c)) is approximately the same as that of the half-sine pulse at half the frequency ratio. For example, whereas the response to the half-sine is a minimum at a frequency ratio of approximately 5, the minimum rise time for the quarter-sine response is at a frequency ratio of approximately 2.5. The oscillation in the quarter-sine response at frequency ratios greater than 2.5 appears to have definite minimums which occur at frequency ratios roughly half those associated with the oscillation in the half-sine pulse. The differences between the rise times of the accelerometer response to the various input pulse shapes are better illustrated in figure 14 where data are presented for $m_1/m_2 = 100$ and $\zeta = 0.01$. No data are presented for the rectangular pulse since the rise time for that input pulse is zero.

Figure 12 shows that over the test range of damping ratios, the effect of damping on the response rise time is negligible for the input pulse shapes examined. This negligible damping effect is further substantiated by the good agreement between the present data which include damping and the isolated data derived from references 6 and 10 where no damping was considered.

The total pulse times of the accelerometer response (fig. 13) are a maximum at the lowest examined frequency ratio and decrease with increasing frequency ratio until they become equal to those of the input. The response pulse time is identical to the input pulse time at approximate frequency ratios of 5 for the half-sine pulse, 10 for the triangular pulse, 20 for the quarter-sine pulse, and between 20 and 50 for the rectangular pulse. In the range of frequency ratios between approximately 2 and 4, the half-sine and triangular response times appear to be less than that of the input whereas the rectangular and quarter-sine pulse responses show a slight increase in the total pulse times. As the

frequency ratio is decreased from 2, the magnitude of the total pulse time of the response to the different pulse shapes tends to coincide, as better illustrated in figure 15 which is a composite of the response data for all test pulse shapes. At a frequency ratio of 0.1, the duration of the response pulse becomes independent of the input and, as expected from the frequency ratio, is 10 times longer than that of the input pulse. If the duration of the response pulse is independent of the shape of the input, then, by definition, it must be equal to the reciprocal of its natural frequency.

The effect of damping on the response pulse time can be determined from figure 13 by comparing the data for the two test damping ratios. Damping only slightly affects the response time and this effect appears to exist only over a range of frequency ratios between approximately 2 and 6. With an increase in the damping, the response pulse duration appears to more closely duplicate the duration of the input force.

Application of Results

Boundaries for application.- The boundaries for application were based upon somewhat arbitrarily selected criteria which fixed the extent to which the accelerometer assembly motions were permitted to affect the impacting body response and still provide acceleration data from which the input forcing function could be inferred. The suitability of these criteria is illustrated in figure 16 which presents the nondimensionalized characteristics of the accelerometer response to a half-sine input pulse as a function of frequency ratio for four mass ratios ranging from 100 to 1. The figure is composed of curves which fair the data over the entire range of frequency ratio. Boundary points for each mass ratio are noted on the curve which is faired through the data for a mass ratio of 100, which, according to figures 11 to 13, corresponds to a mass ratio of infinity. These boundary points were taken from figure 6(a) and denote the frequency ratio which separates acceptable from unacceptable impacting body accelerations according to the selected criteria. At frequency ratios below that for each boundary point, the impacting body response was judged unacceptable. Figure 16 shows that the response characteristics for a given mass ratio deviate from those described by a mass ratio of 100 at a frequency ratio which, in general, is somewhat less than that for the corresponding boundary point. This trend prevails for all mass ratios and all input pulses and indicates that the selected criteria produced slightly conservative boundaries for application since the boundary points could have been extended to somewhat lower frequency ratios and still provide an accelerometer response from which the input forcing function could be inferred.

Since the boundaries for application define a range of system parameters for which the accelerometer assembly response is the same as that for a system having an infinite mass ratio, the impact response characteristics can be evaluated from a single-degree-of-freedom analysis. In effect, these boundaries define conditions which extend the

applicability of a single-degree-of-freedom analysis to describe a two-degree-of-freedom system.

Applied to a penetrometer-type system, these boundaries for application define parameters of the system where the accelerometer assembly and its mount do not affect the motions of the impacting body beyond prescribed limits and for which a single-degree-of-freedom analysis is appropriate. In addition, these boundaries have application to determine the effects on the impacting body of other flexibly mounted masses.

Acceleration time histories.- The results of this study have shown that the acceleration time histories of an accelerometer assembly mounted to an impacting body are dependent upon factors which include characteristics of the coupling and the shape of the input pulse applied to the impacting body. If the impact data collected from the acceleration sensor of a penetrometer-type device is to be meaningful, it must reflect the input forces applied by the target material to the impacting body. More specifically, for penetrometer applications it is necessary that the input acceleration time history be definable from the acceleration time history recorded by the accelerometer sensor and from a knowledge of the system parameters including the impact velocity.

To determine the input forcing function from the accelerometer assembly acceleration time history, it is necessary to first establish ω, the frequency associated with the duration of the input force. This frequency fixes the frequency ratio which permits the application of the results of this paper. Figure 17 is a composite of data for the examined pulse shapes taken from figure 15 which relates the frequency of the input pulse ω to a frequency based upon the duration of the accelerometer assembly acceleration time history. This latter frequency ω' is defined as $\omega' = \pi/t_t$. In figure 17 the undamped natural frequency of the accelerometer assembly ω_n is divided by ω' and plotted as a function of ω_n/ω, the frequency ratio. When $\omega = \omega'$, shown by the dashed line, the total pulse time of the accelerometer response t_t is equal to the duration of the input pulse t_T. The frequency ω' is immediately available from the accelerometer response and the ratio ω_n/ω' reveals significant information toward the definition of the input pulse. This figure shows that ω equals ω' at all frequency ratios greater than approximately 8 and for all pulse shapes. Damping for the system shown is 0.01; however, for more highly damped systems, ω equals ω' at frequency ratios which are only slightly lower. (See fig. 13.) As shown by the sketches in this figure and the acceleration time histories of figure 8, for values of ω_n/ω' between approximately 8 and 50, the input forcing function is readily inferred from the acceleration time history of the accelerometer since, over this range of the ratio, the response can be faired by the input pulse. At ratios greater than 50, the accelerometer support structure is sufficiently stiff that the accelerometer assembly effectively is rigidly attached to the impacting body and the acceleration time history of the accelerometer is the same as that of the input function for half-sine,

triangular, and quarter-sine pulse shapes. The rectangular input function at these higher ratios depends upon a fairing of the response for definition since, as shown in figure 8(d), the step change in acceleration results in response oscillations at all frequency ratios above 2.

For values of ω_n/ω' below approximately 8 where ω' differs from ω, the input force is not easily inferred solely from the shape of the accelerometer response, particularly at ratios below 2 where the shape of the response is similar for all inputs. (See fig. 8.) To describe the input forcing function in this range of ω_n/ω' requires a measurement of the magnitude of the accelerometer response characteristics and the application of the results of the analytical studies of this paper. An iteration procedure is necessary for this description which consists of assuming a frequency ratio, relating the accelerometer response characteristics to the corresponding characteristics of each input pulse (computed with the aid of the known impact velocity since the area under the input acceleration time history equals the impact velocity), and comparing these ratios to those obtained analytically (as, for example, the data of figs. 11, 14, and 15). The initial frequency-ratio assumption required in this range of ω_n/ω' is simplified by an examination of the shape of the response acceleration time history. If the response is smooth – that is, without superimposed oscillations (sketch at $\omega_n/\omega = 0.5$ in fig. 17) – then the frequency ratio is equal to or less than 2. (Obviously, smooth responses also result from input pulses without step changes at high values of ω_n/ω' (above 50).) Should the response contain oscillations, the frequency ratio is greater than 2 – the value of the ratio depending upon the number of oscillations – as shown in figure 8.

CONCLUDING REMARKS

An analytical investigation was performed to study the dynamic response to impact loadings of acceleration sensors having various mounting characteristics. The following remarks are based upon the results of this investigation.

Boundaries for the system parameters were established that defined conditions for which the accelerometer assembly and its coupling have a negligible effect on the accelerations experienced by an impacting body subjected to half-sine, triangular, quarter-sine, and rectangular input pulses. These boundaries, based upon criteria selected consistent with the accuracy of present-day shock-measuring accelerometers and recording systems, define ranges of the test parameters of the two-degree-of-freedom system for which the impact response characteristics can be evaluated from a single-degree-of-freedom analysis.

The peak accelerations of the response to the various input pulses vary differently with frequency ratio (the ratio of the accelerometer assembly undamped natural frequency

to the frequency corresponding to the duration of the input pulse). The maximum response acceleration, which exceeds the maximum input acceleration, occurs within a frequency-ratio range between 1 and 2, decreases toward zero at lower ratios, and, except for the rectangular pulse, decreases to that of the input at higher ratios. The response peak acceleration to a rectangular input pulse reaches a maximum at a frequency ratio of 1 and is unchanged for all higher frequency ratios. Characteristic times of the response decrease from a maximum at the lowest examined frequency ratio, where they are independent of the pulse shape, and approach those of the input at frequency ratios below 50 for the rise times and below approximately 20 for the total pulse times. The presence of damping in the mounting system decreases the magnitude of the peak acceleration and has a negligible effect upon the characteristic times of the accelerometer response.

With a knowledge of the system parameters and the impact velocity, the shape and magnitude of the input pulse applied to an impacting body can be deduced from characteristics of the acceleration-time-history response of an accelerometer assembly mounted to that body. The ratio of the undamped natural frequency of the accelerometer assembly to the frequency associated with the total pulse time of the accelerometer assembly response is a significant factor in this deduction. For values of this ratio greater than approximately 50, the acceleration time history of the acceleration sensor is the same as that of the input forcing function for half-sine, triangular, and quarter-sine pulse shapes. At ratios between approximately 8 and 50, the input forcing function is readily inferred from the response acceleration time history since the latter can be faired by the input pulse. The rectangular input function is inferred from a fairing of the response for all ratios above 8. For values of this ratio below 8, characteristics of all examined input functions can be inferred; however, the task is somewhat tedious, employing a simple iteration procedure which requires comparisons between conjectured response characteristics and those obtained from the analytical study.

Langley Research Center,
National Aeronautics and Space Administration,
Langley Station, Hampton, Va., December 22, 1966,
124-08-04-01-23.

REFERENCES

1. McCarty, John Locke; Beswick, Alfred G.; and Brooks, George W.: Penetrometer Techniques for Lunar Surface Evaluation. A Compilation of Recent Research Related to the Apollo Mission, NASA TM X-890, 1963, pp. 123-130.

2. McCarty, John Locke; Beswick, Alfred G.; and Brooks, George W.: Application of Penetrometers to the Study of Physical Properties of Lunar and Planetary Surfaces. NASA TN D-2413, 1964.

3. Beswick, Alfred G.; and McCarty, John Locke: Penetrometer Research and Development for Lunar Surface Evaluation. Conference on Langley Research Related to Apollo Mission, NASA SP-101, 1965, pp. 61-68.

4. McCarty, John Locke; and Carden, Huey D.: Impact Characteristics of Various Materials Obtained by an Acceleration-Time-History Technique Applicable to Evaluating Remote Targets. NASA TN D-1269, 1962.

5. Hanks, Brantley R.; and McCarty, John Locke: Investigation of the Use of Penetrometers To Determine the Capability of Dust Materials To Support Bearing Loads. NASA TN D-3200, 1966.

6. Frankland, J. M.: Effects of Impact on Simple Elastic Structures. Rept. 481, David W. Taylor Model Basin, U.S. Navy, Apr. 1942.

7. Biot, M. A.; and Bisplinghoff, R. L.: Dynamic Loads on Airplane Structures During Landing. NACA WR W-92, 1944. (Formerly NACA ARR 4H10.)

8. Jacobsen, Lydik S.; and Ayre, Robert S.: Engineering Vibrations. McGraw-Hill Book Co., Inc., 1958.

9. Kornhauser, M.: Structural Effects of Impact. Spartan Books, Inc., c.1964, pp. 61-95.

10. Levy, Samuel; and Kroll, Wilhelmina D.: Response of Accelerometers to Transient Accelerations. Res. Paper 2138, J. Res. Natl. Bur. Std., vol. 45, no. 4, Oct. 1950, pp. 303-309.

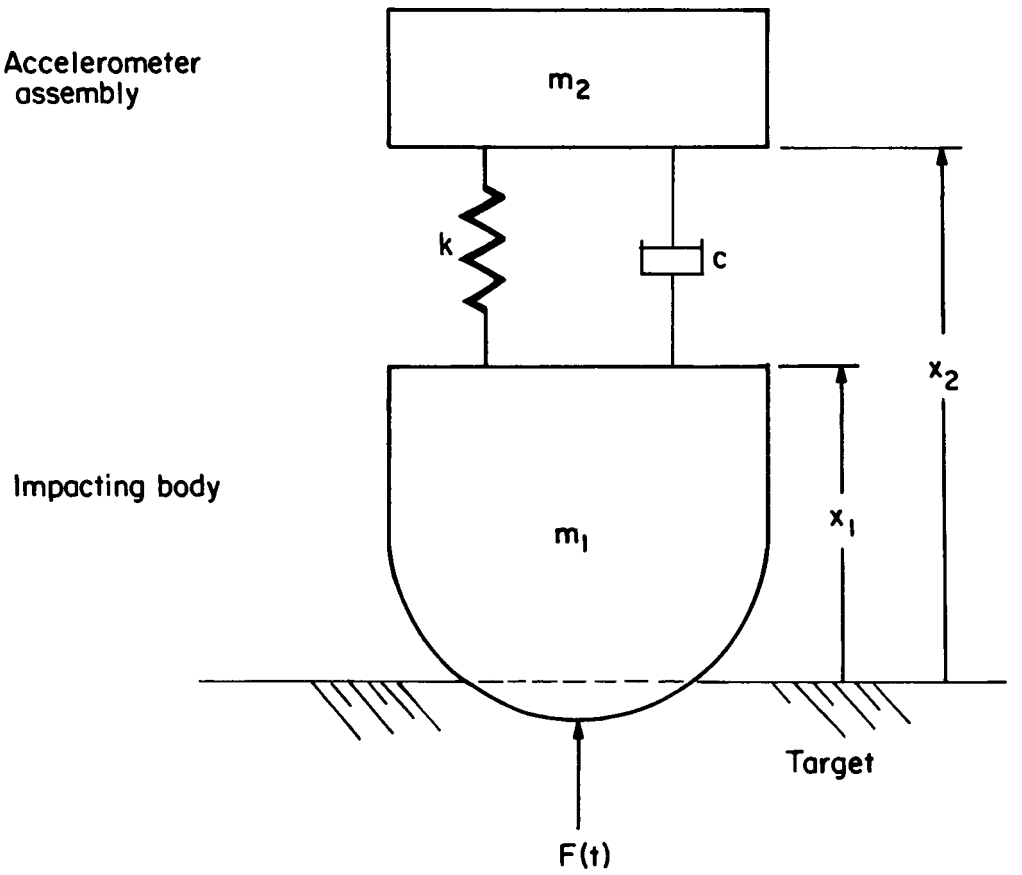

Figure 1.- Schematic of system used in analysis.

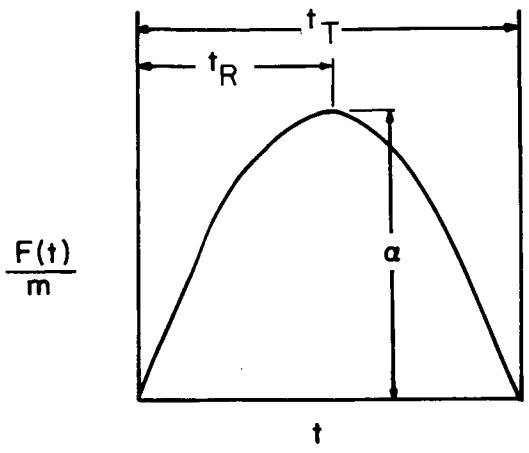

(a) Half-sine input.

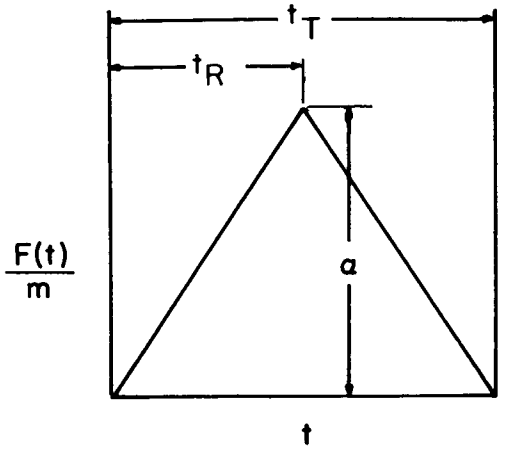

(b) Triangular input.

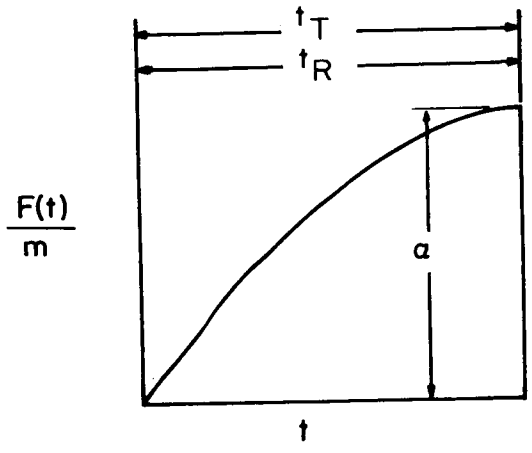

(c) Quarter-sine input.

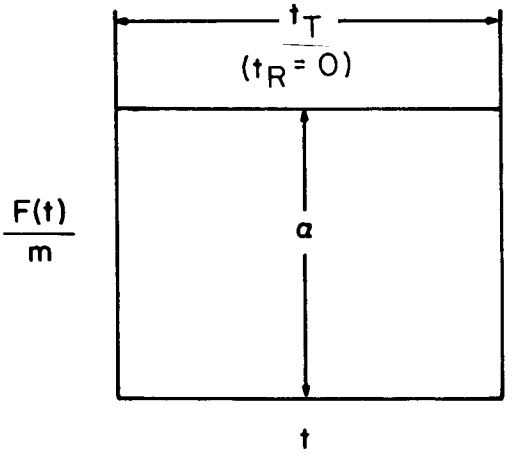

(d) Rectangular input.

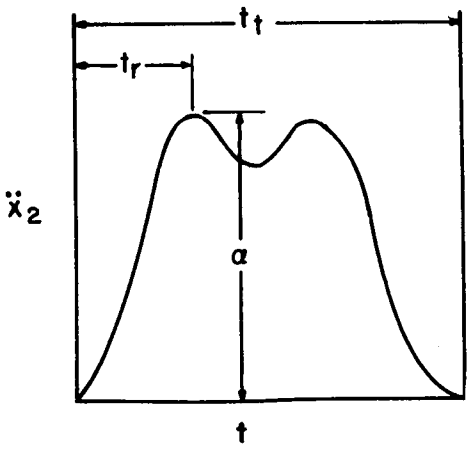

(e) Sample accelerometer response.

Figure 2.- Input acceleration pulse shapes and sample accelerometer response showing nomenclature.

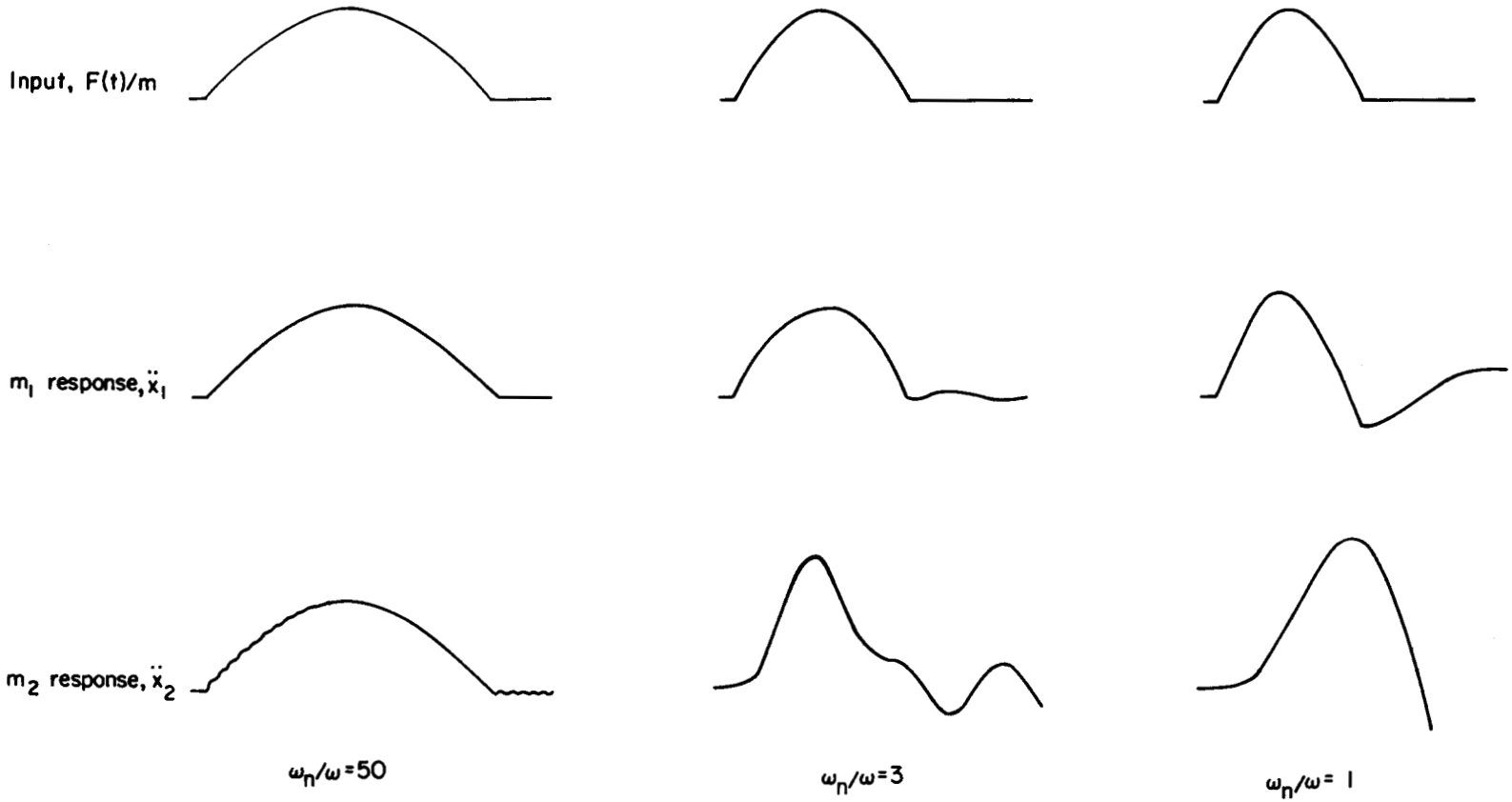

(a) $m_1/m_2 = 5$.

Figure 3.- Response of masses m_1 and m_2 to half-sine input force at several frequency ratios. $\zeta = 0.01$.

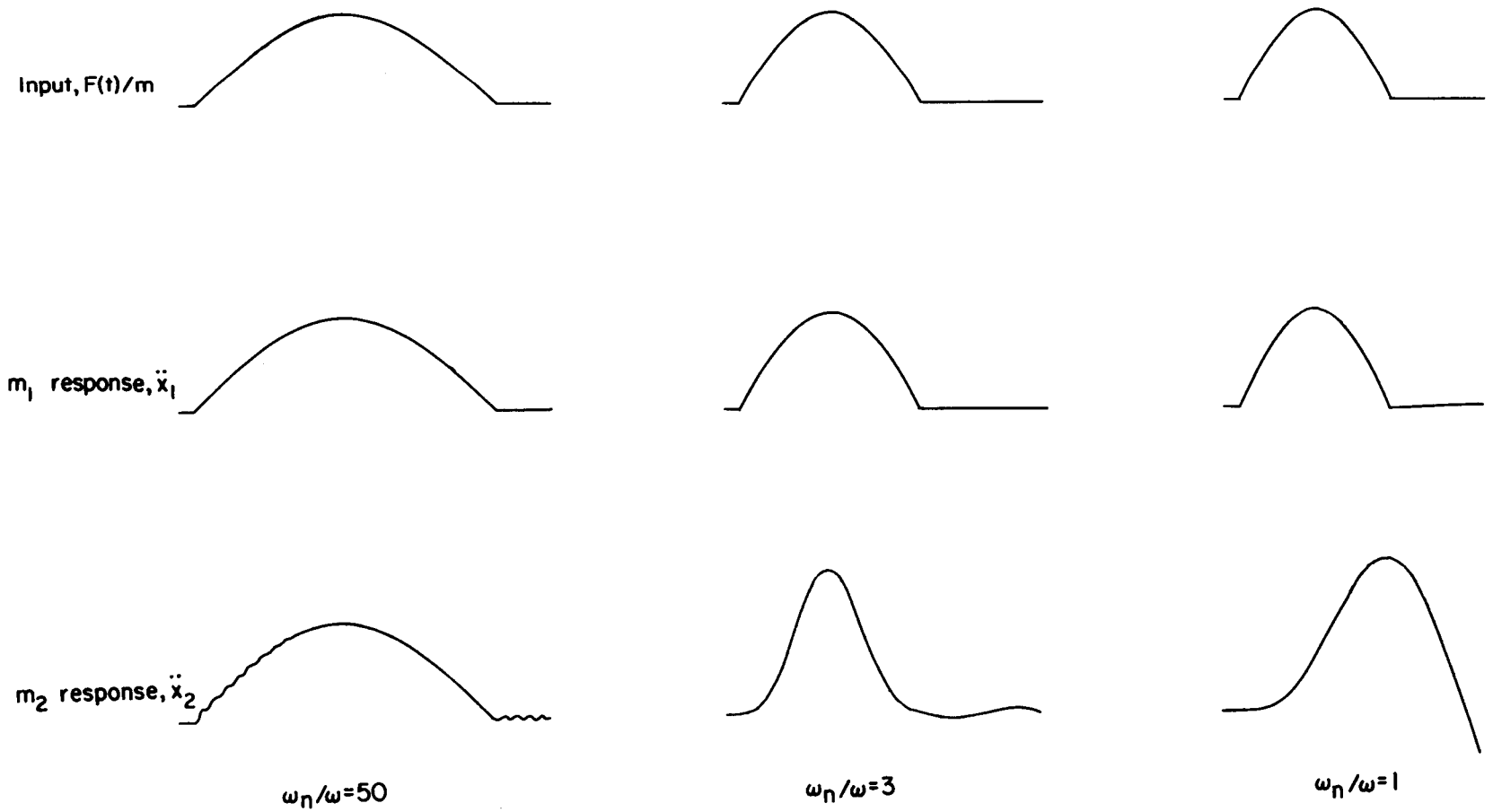

(b) $m_1/m_2 = 100$.

Figure 3.- Concluded.

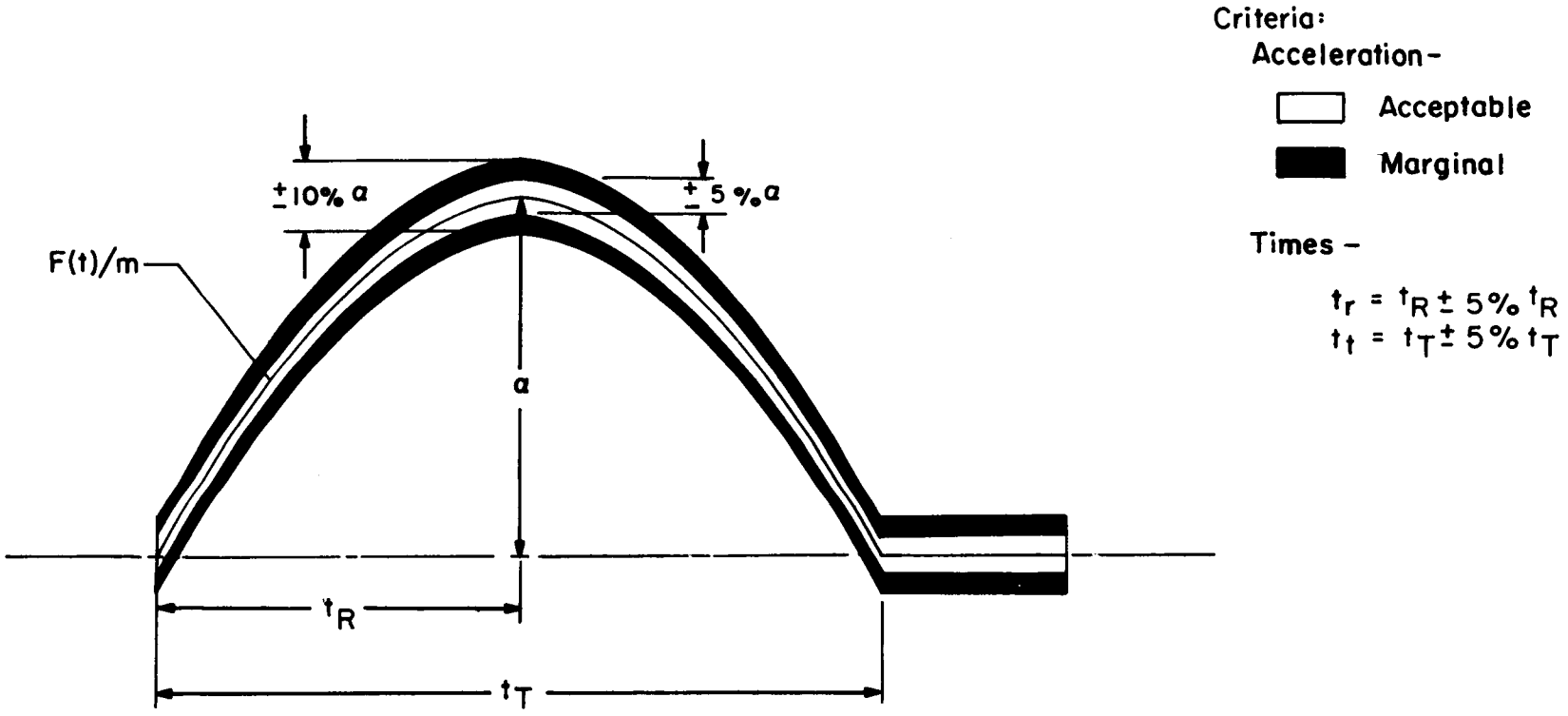

Figure 4.- Criteria for acceptable reproduction of input force acceleration by impacting body.

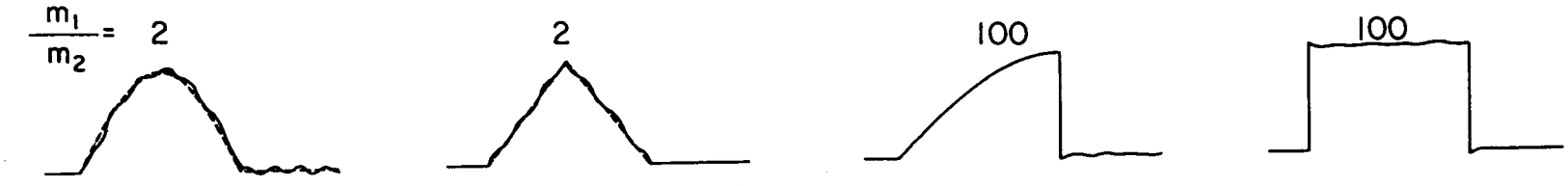

(a) Acceptable.

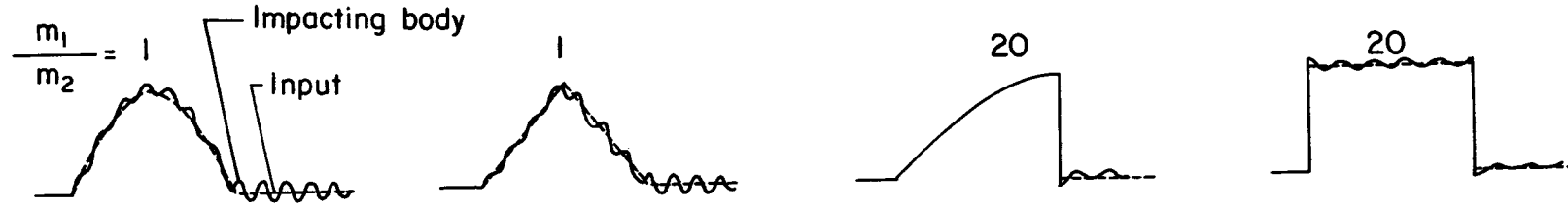

(b) Marginal.

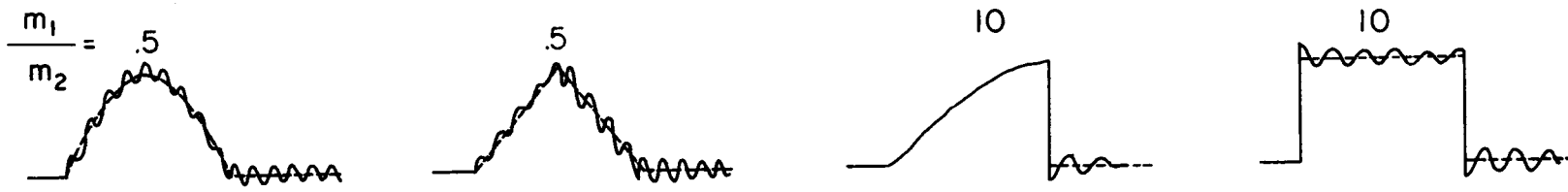

(c) Unacceptable.

Figure 5.- Sample impacting body accelerations $\ddot{x}_1$ illustrating the application of the criteria for acceptability. $\omega_n/\omega = 10$; $\zeta = 0.01$.

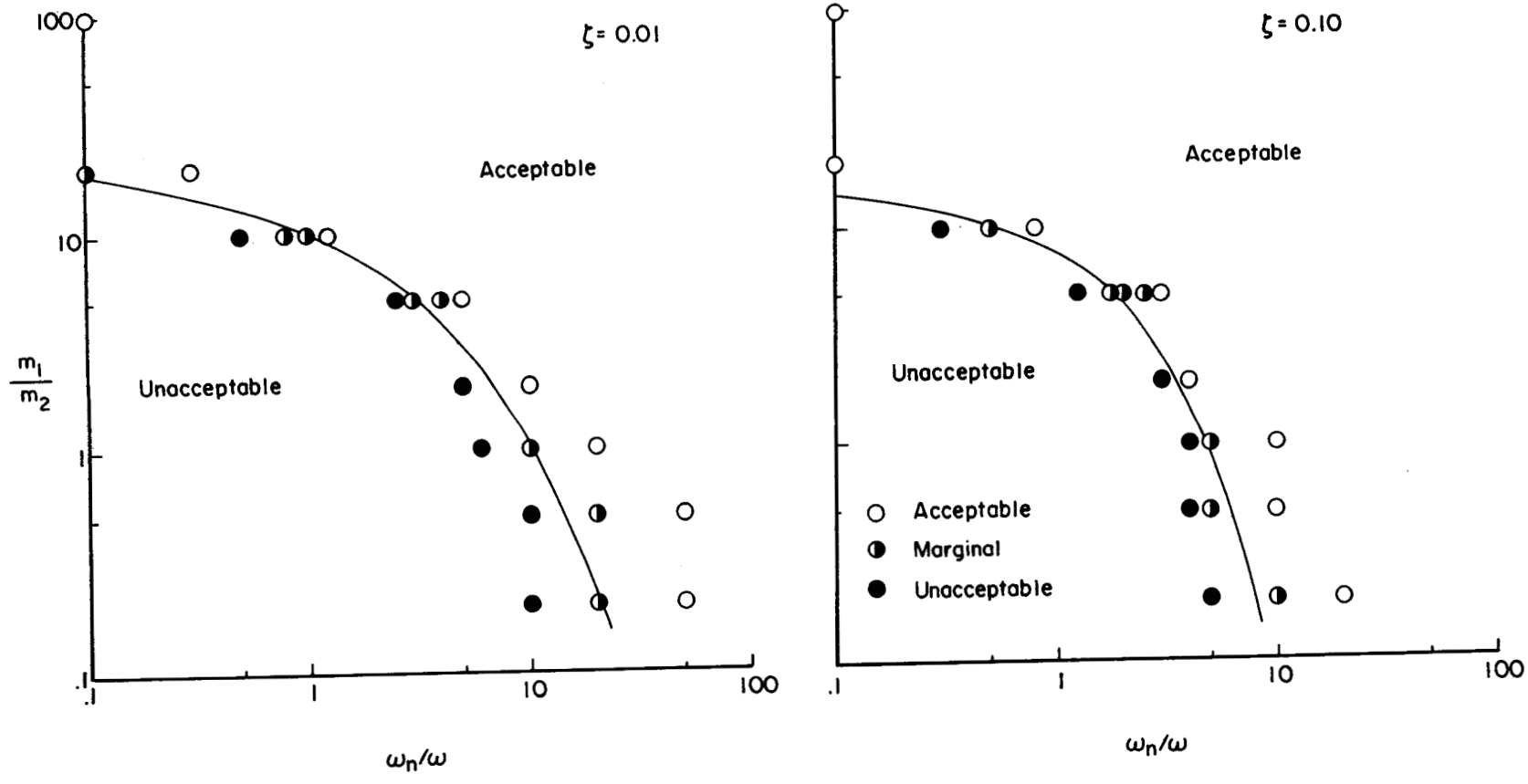

(a) Half-sine pulse.

Figure 6.- Boundaries of system parameters for applicable data based upon selected criteria.

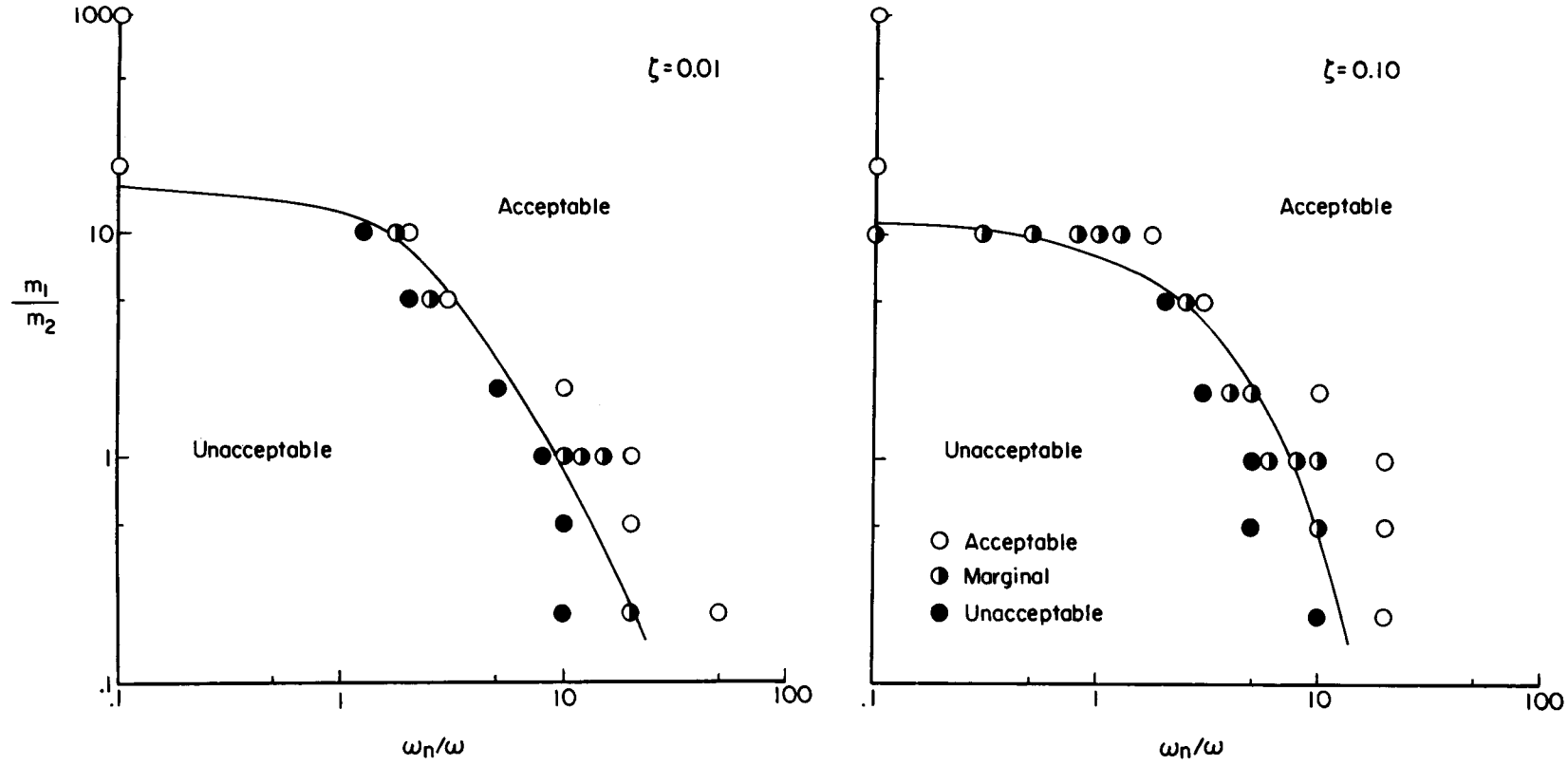

(b) Triangular pulse.

Figure 6.- Continued.

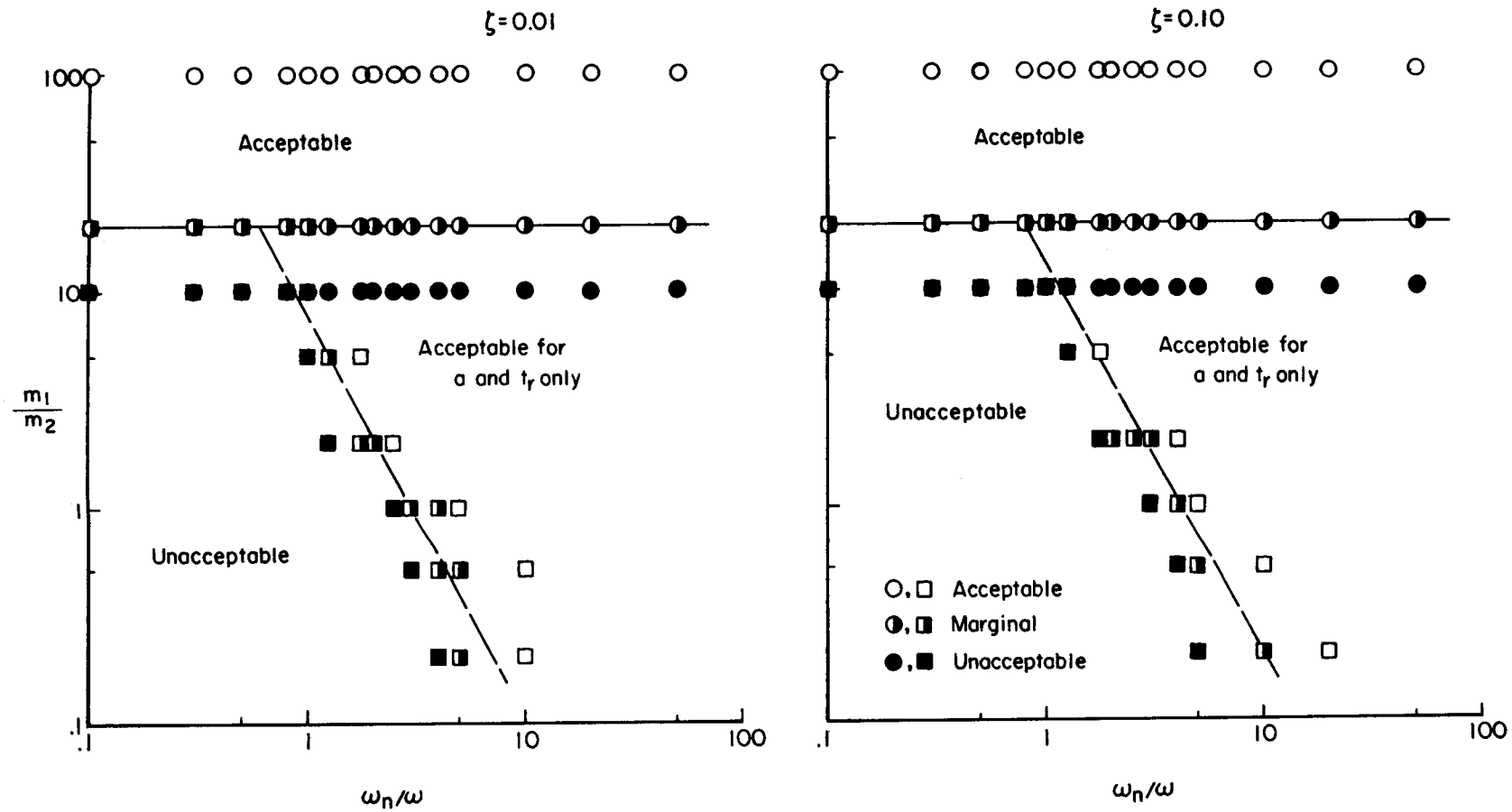

(c) Quarter-sine pulse.

Figure 6.- Continued.

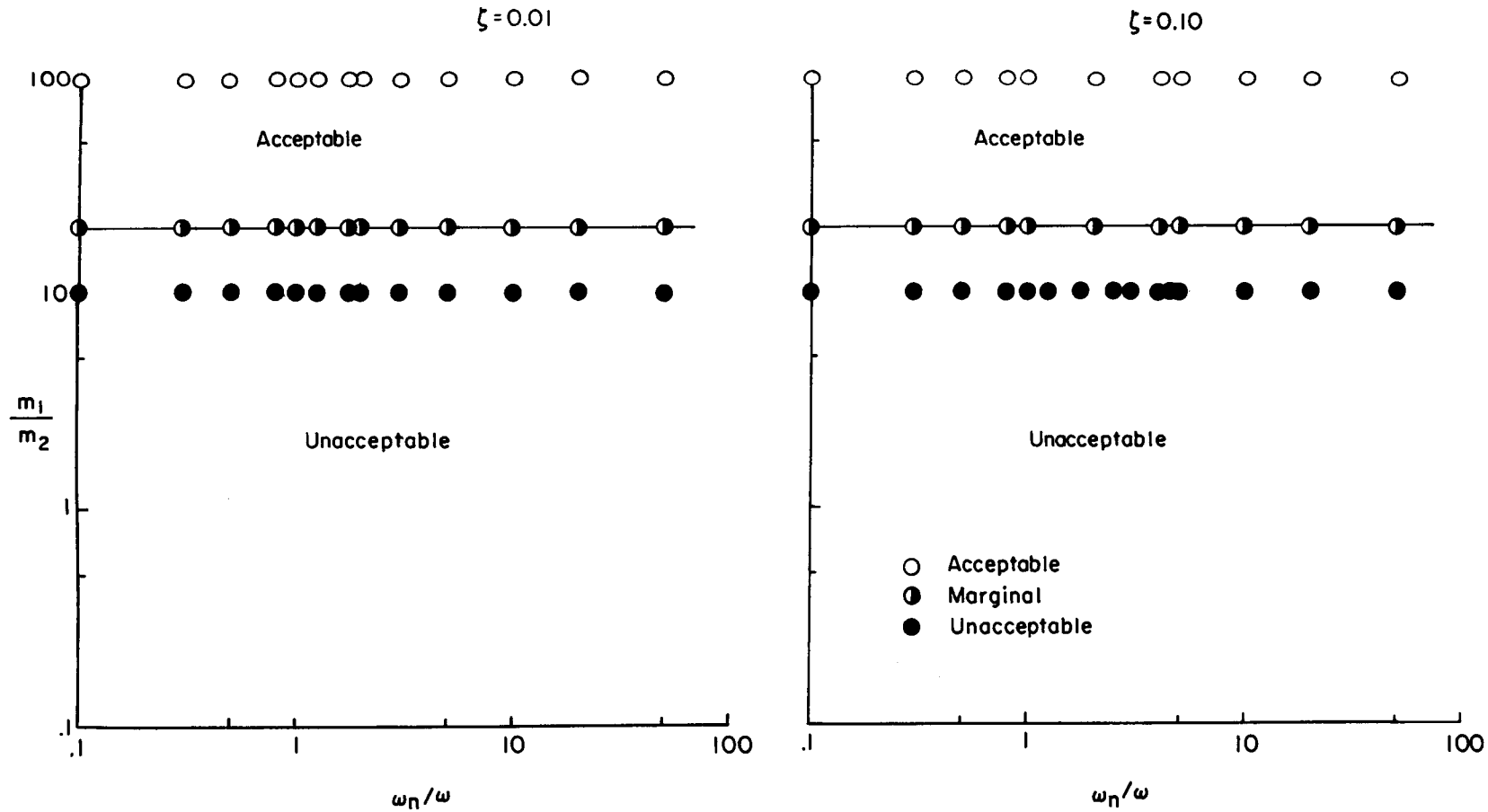

(d) Rectangular pulse.

Figure 6.- Concluded.

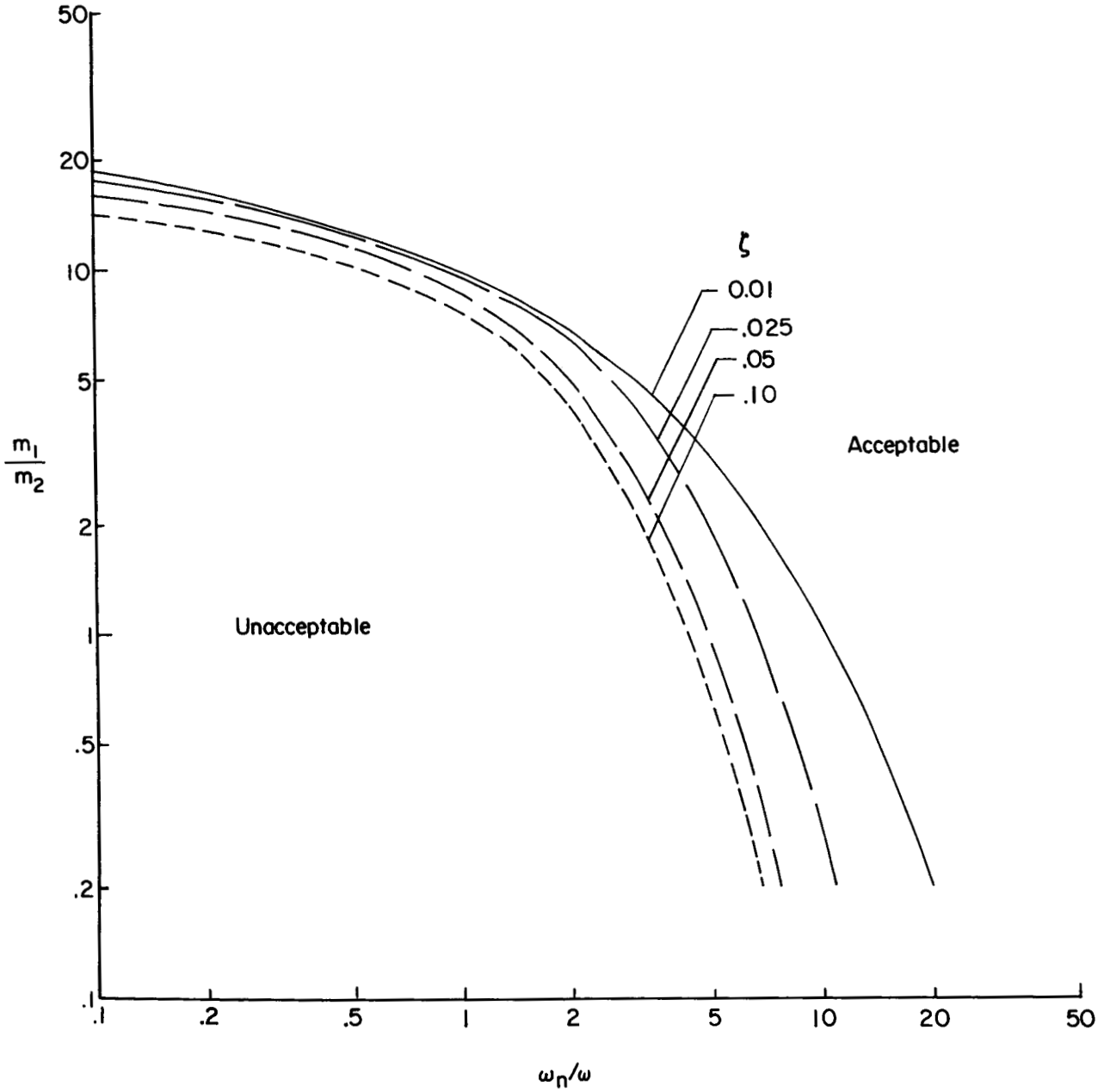

Figure 7.- Effect of damping on boundaries for application. Half-sine pulse.

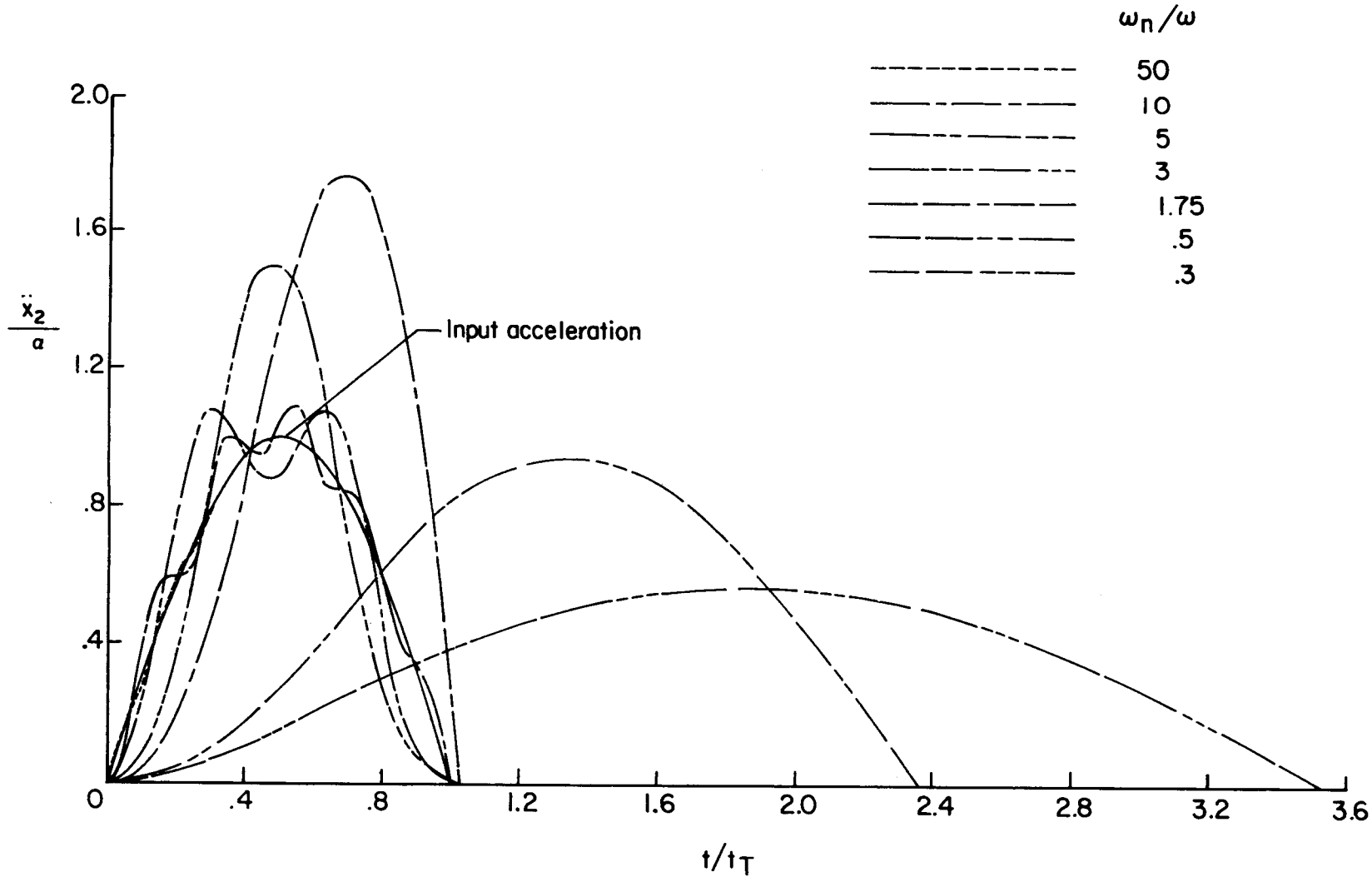

(a) Half-sine pulse.

Figure 8.- Response of accelerometer to various input acceleration pulse shapes for specific frequency ratios ω_n/ω. $m_1/m_2 = 100$; $\zeta = 0.01$.

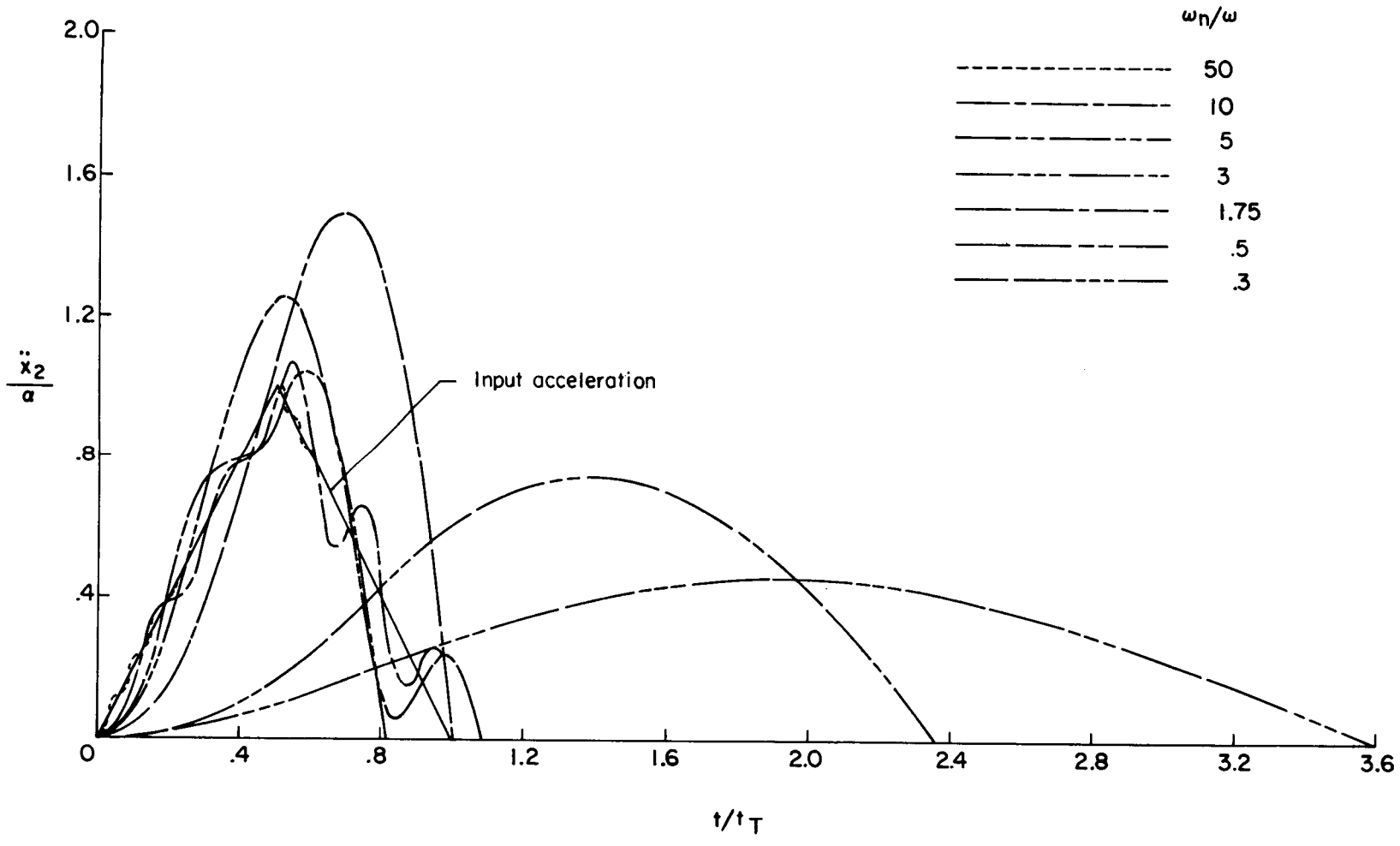

(b) Triangular pulse.

Figure 8.- Continued.

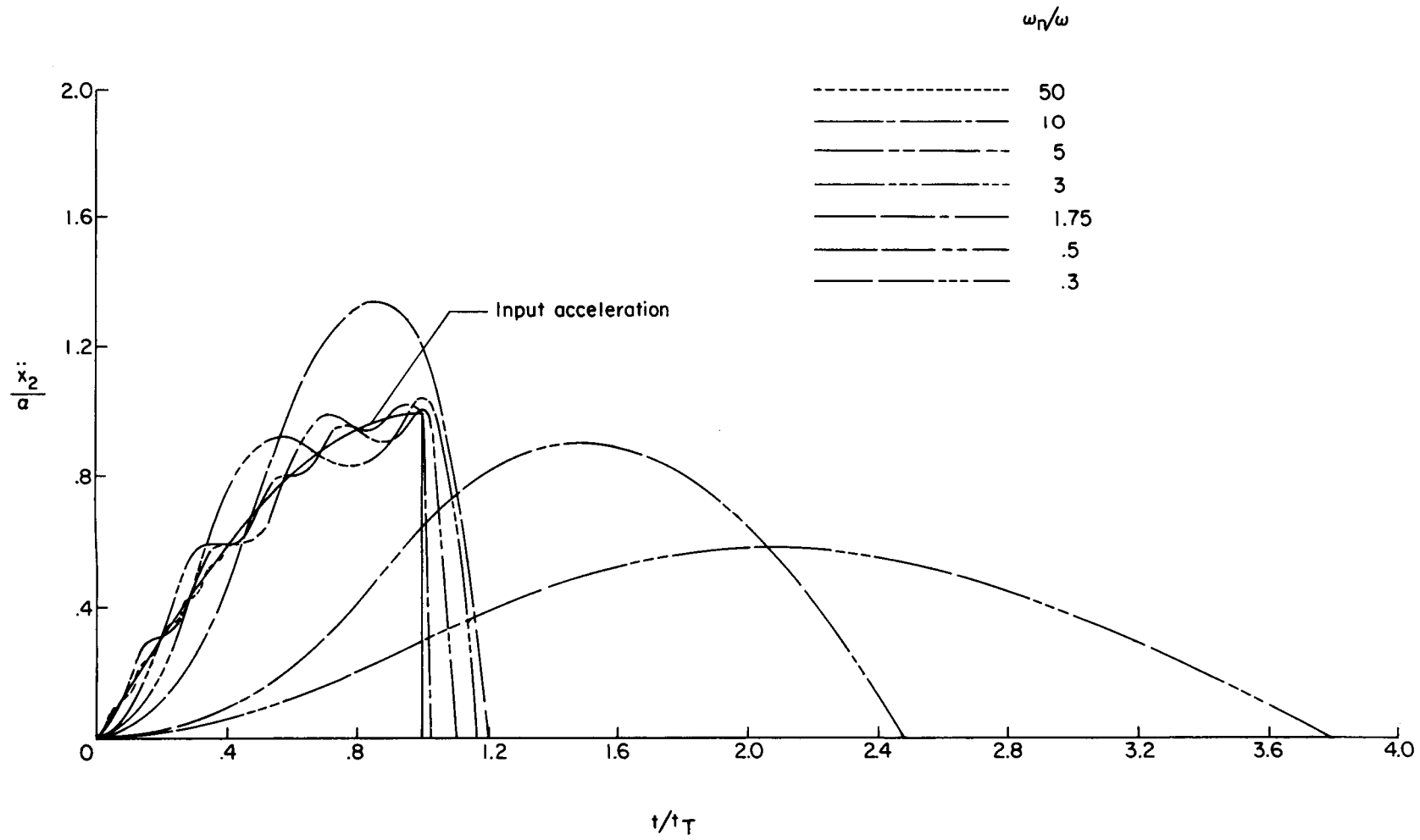

(c) Quarter-sine pulse.

Figure 8.- Continued.

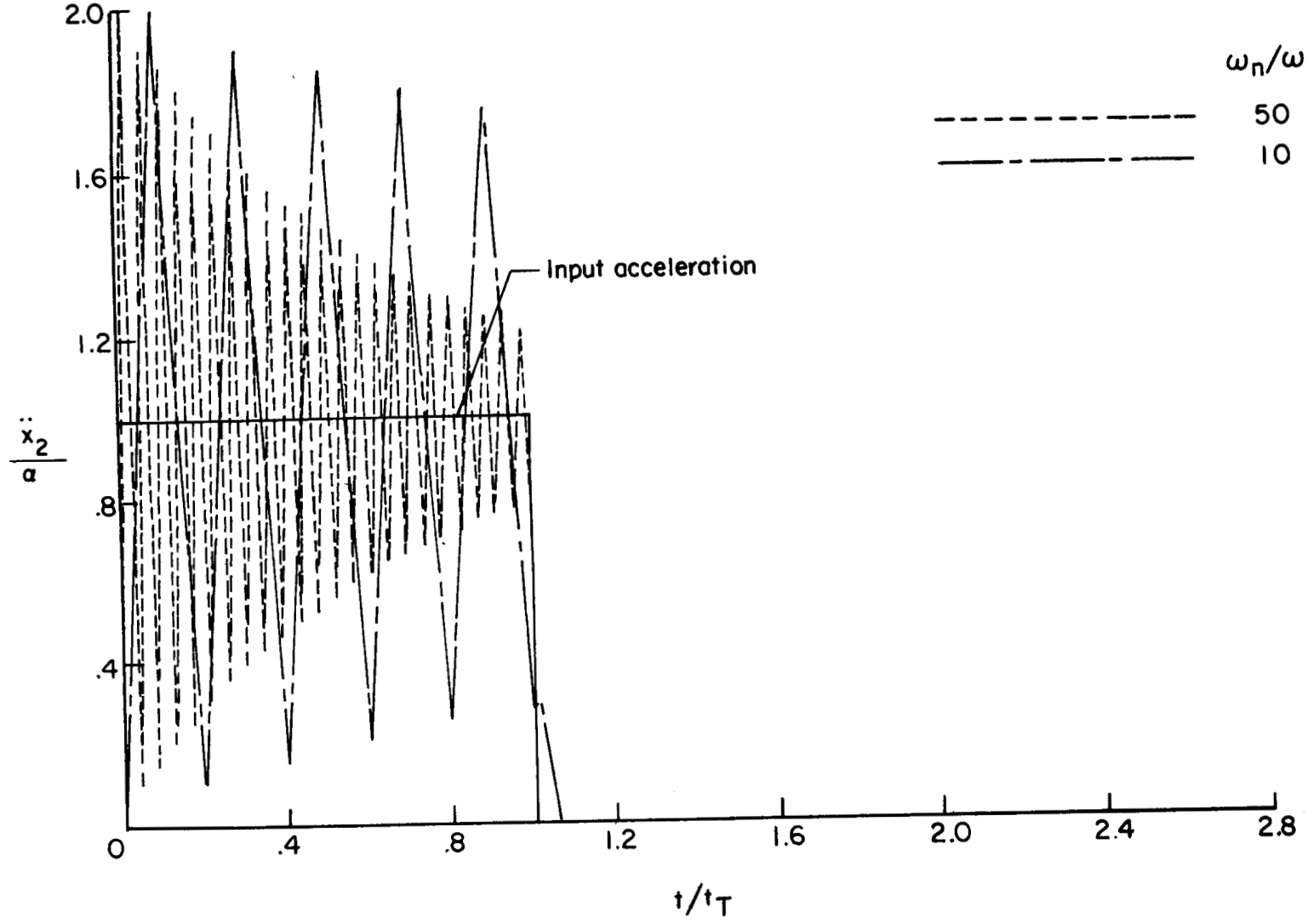

(d) Rectangular pulse.

Figure 8.- Continued.

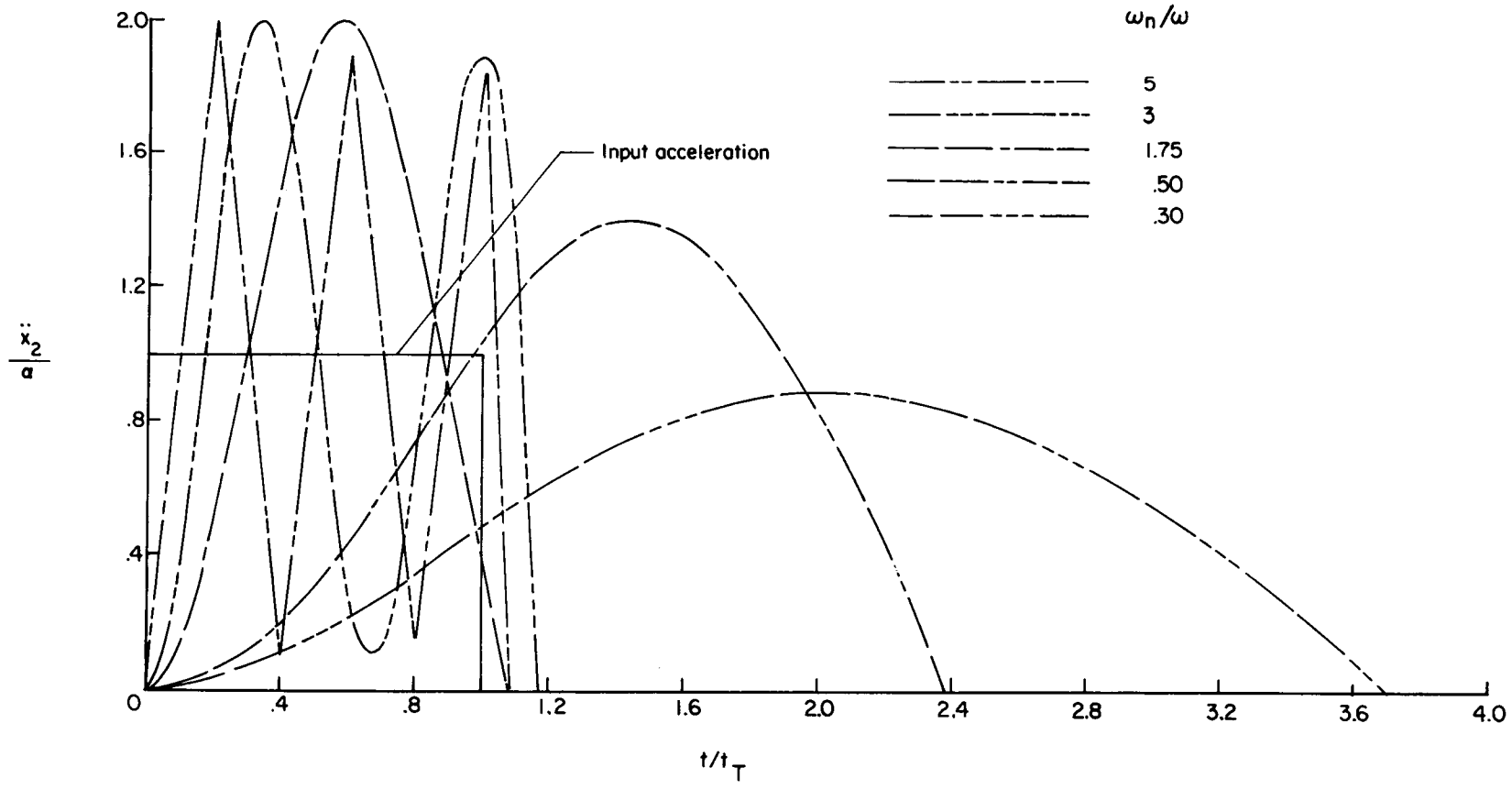

(d) Concluded.

Figure 8.- Concluded.

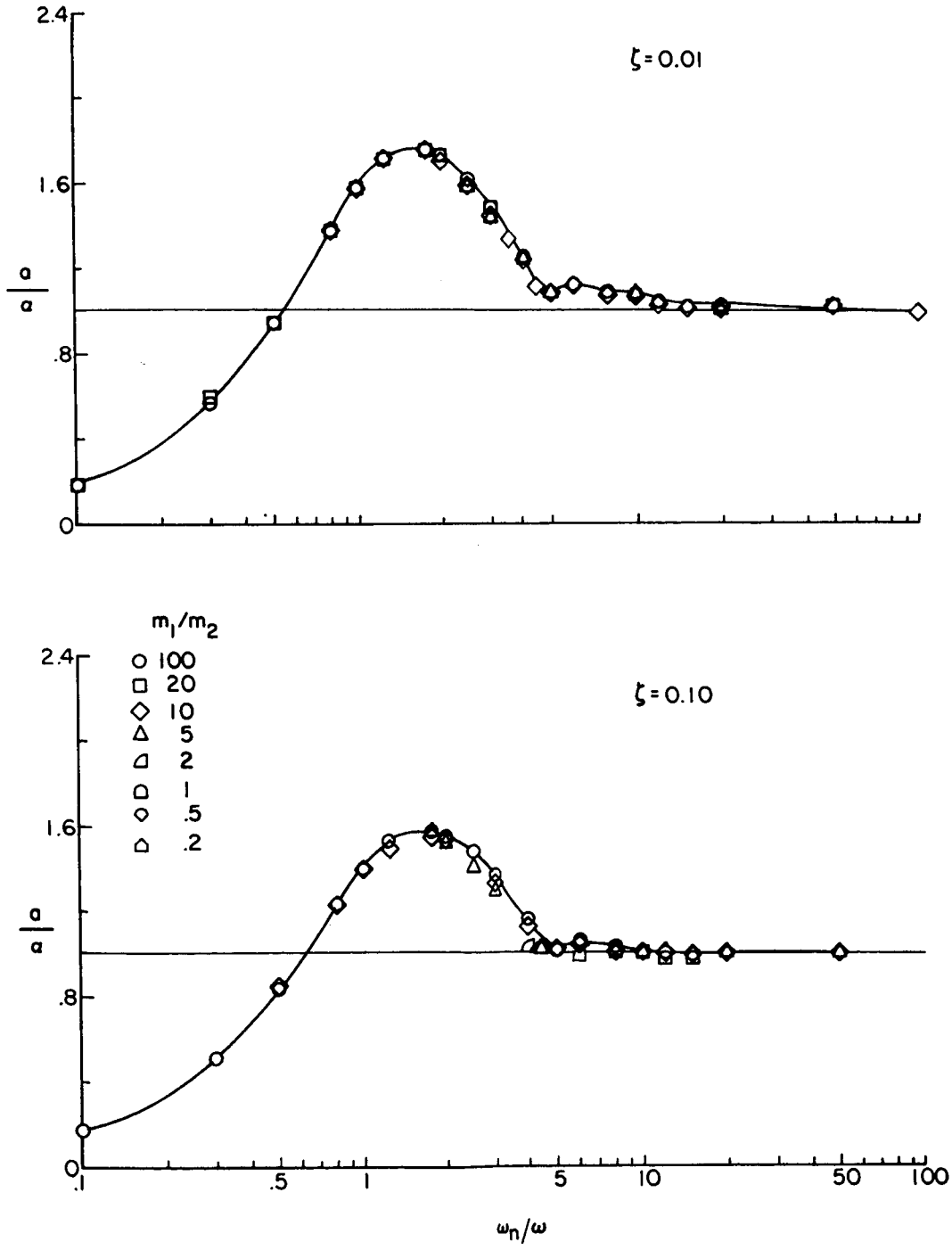

(a) Half-sine pulse.

Figure 9.- Peak acceleration response of accelerometer assembly to various input pulses.

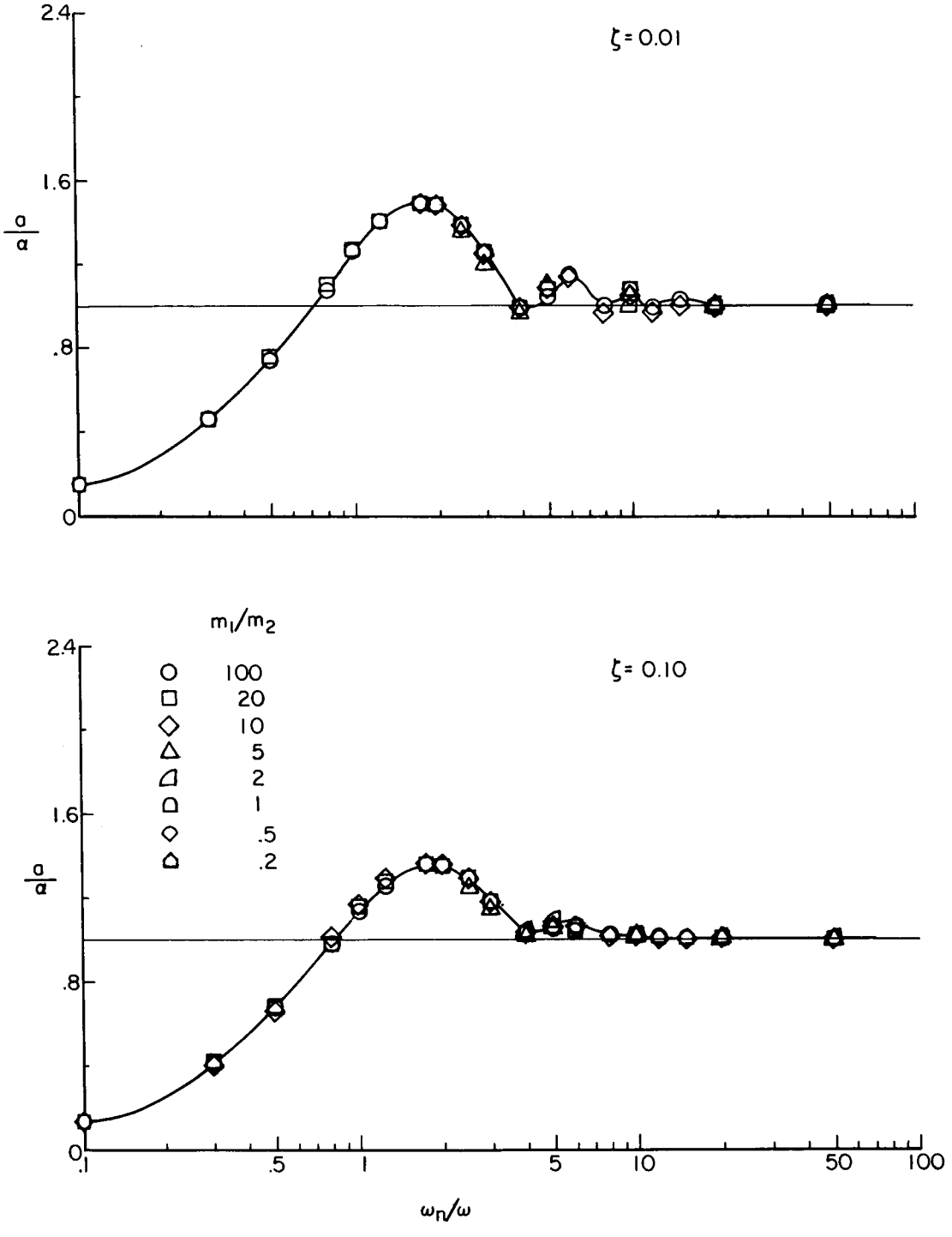

(b) Triangular pulse.

Figure 9.- Continued.

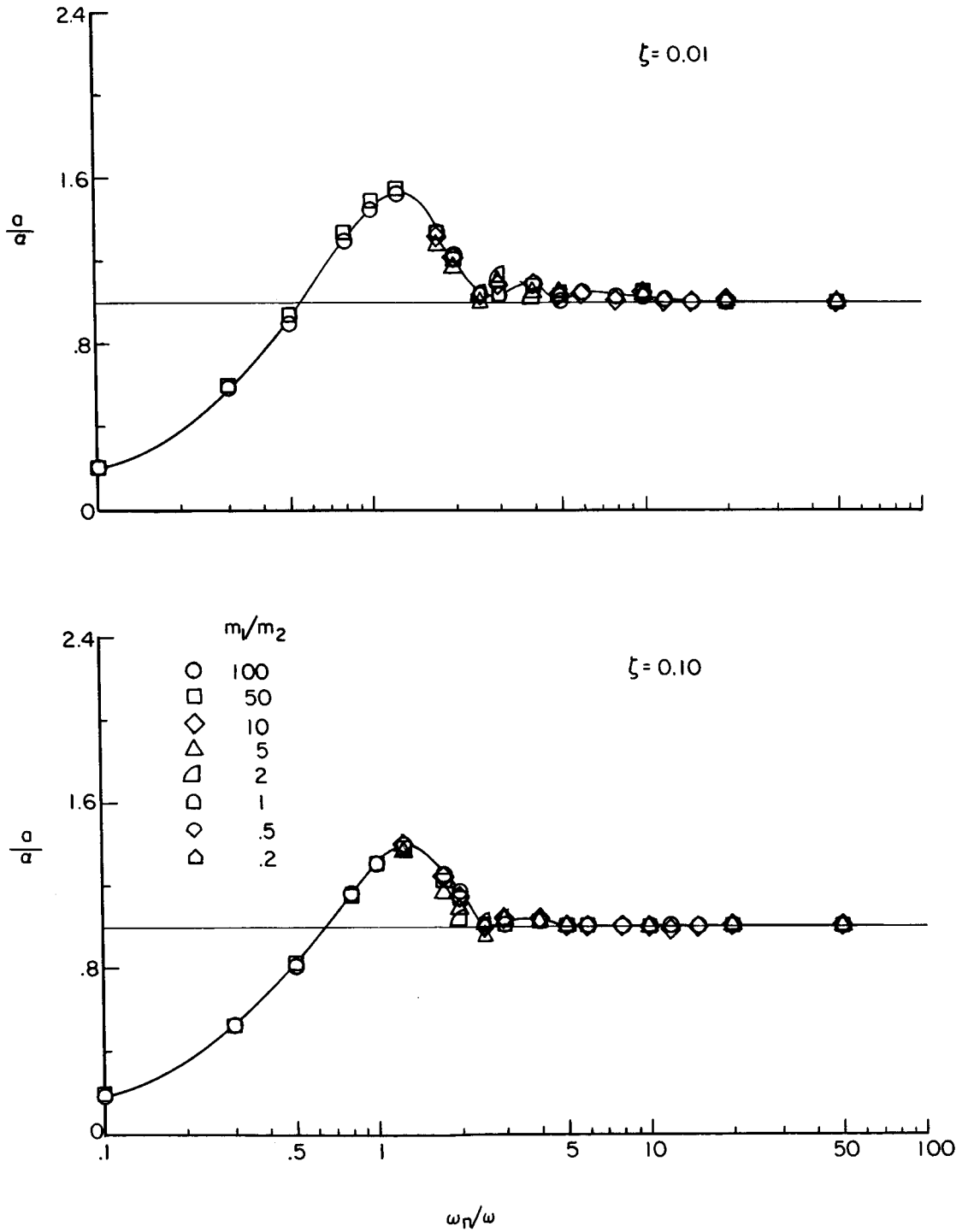

(c) Quarter-sine pulse.

Figure 9.- Continued.

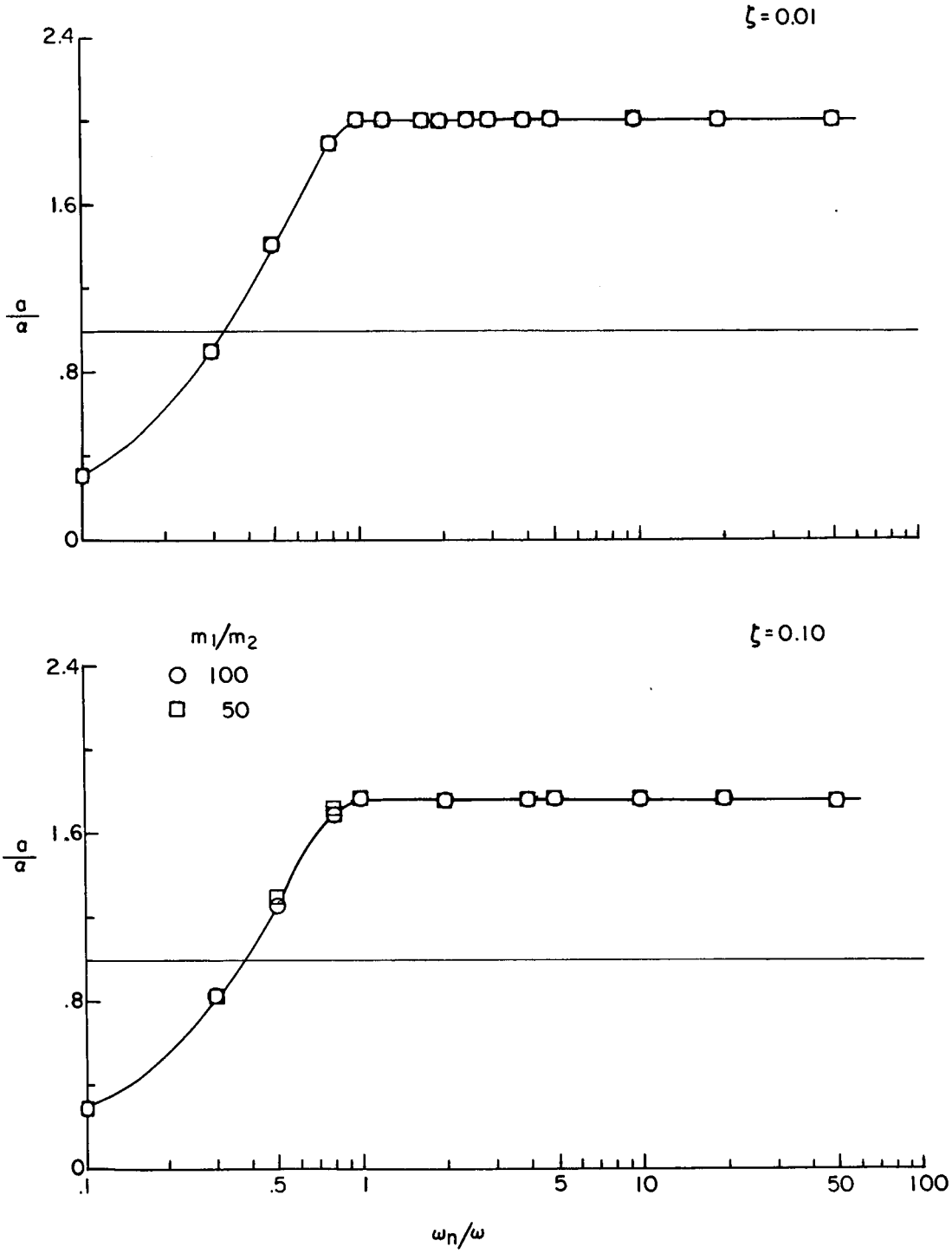

(d) Rectangular pulse.

Figure 9.- Concluded.

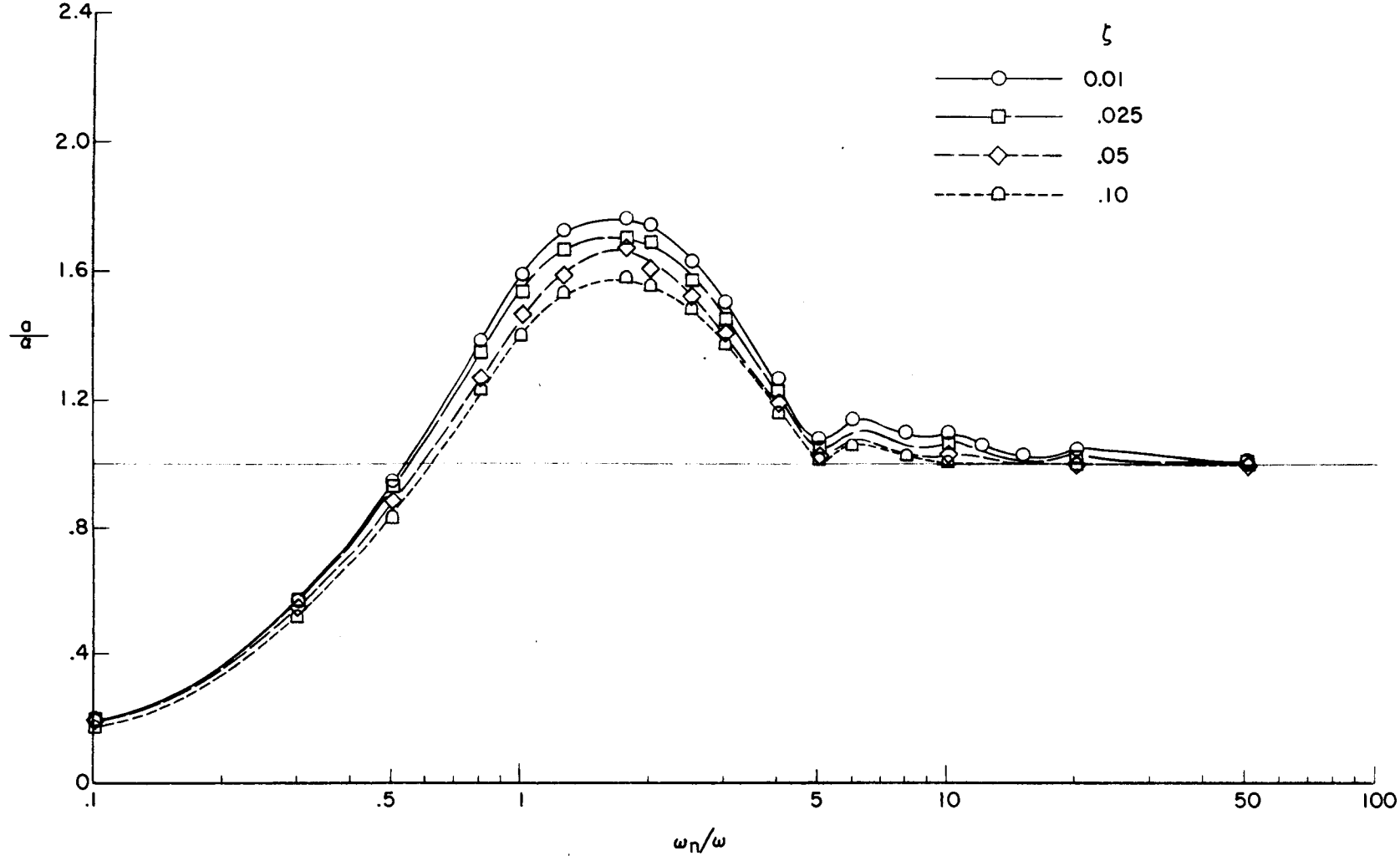

Figure 10.- Effect of damping on peak acceleration response of accelerometer. Half-sine pulse; $m_1/m_2 = 100$.

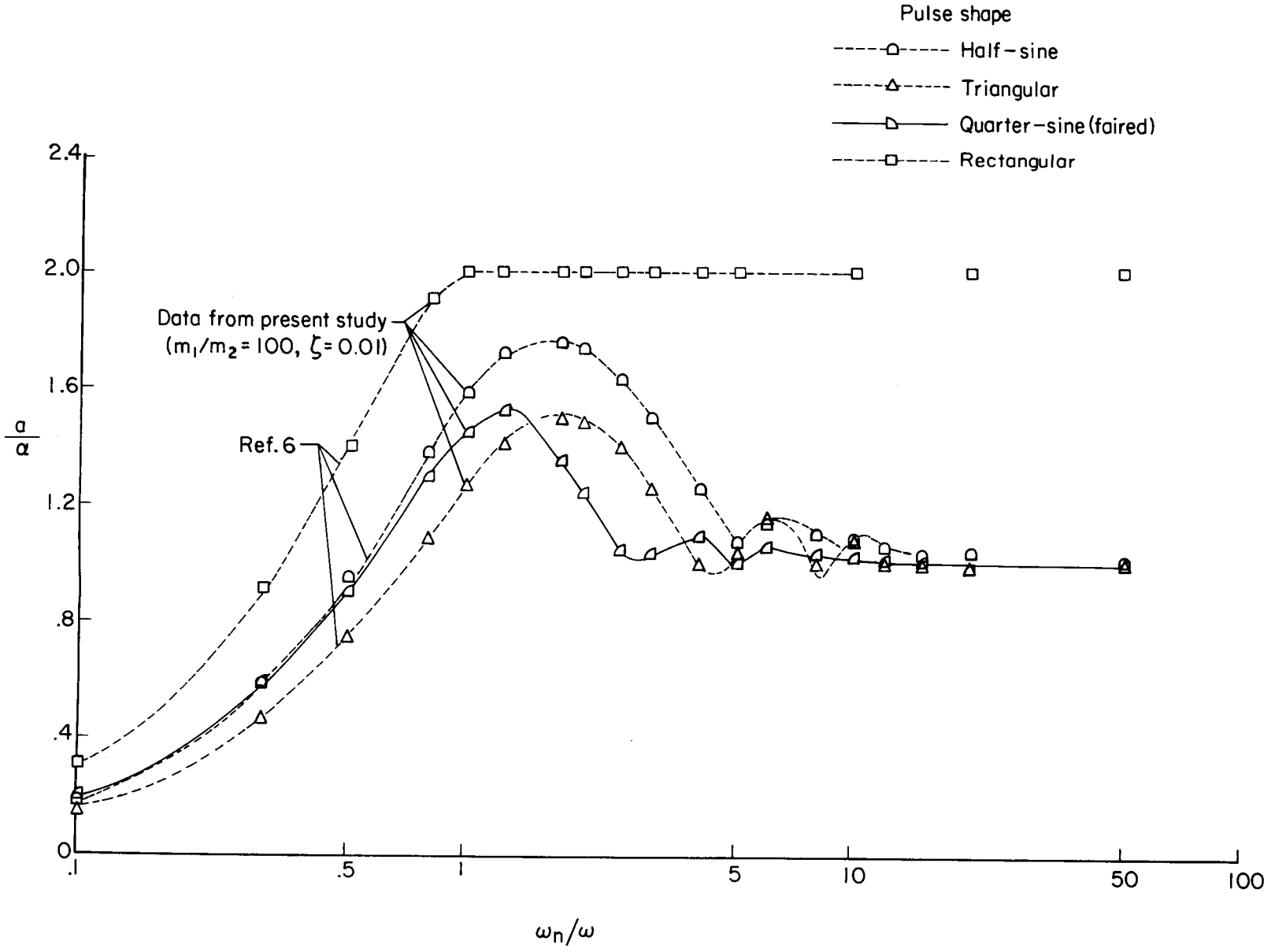

Figure 11.- Peak acceleration response to various pulse shapes with reference data from single-degree-of-freedom analysis.

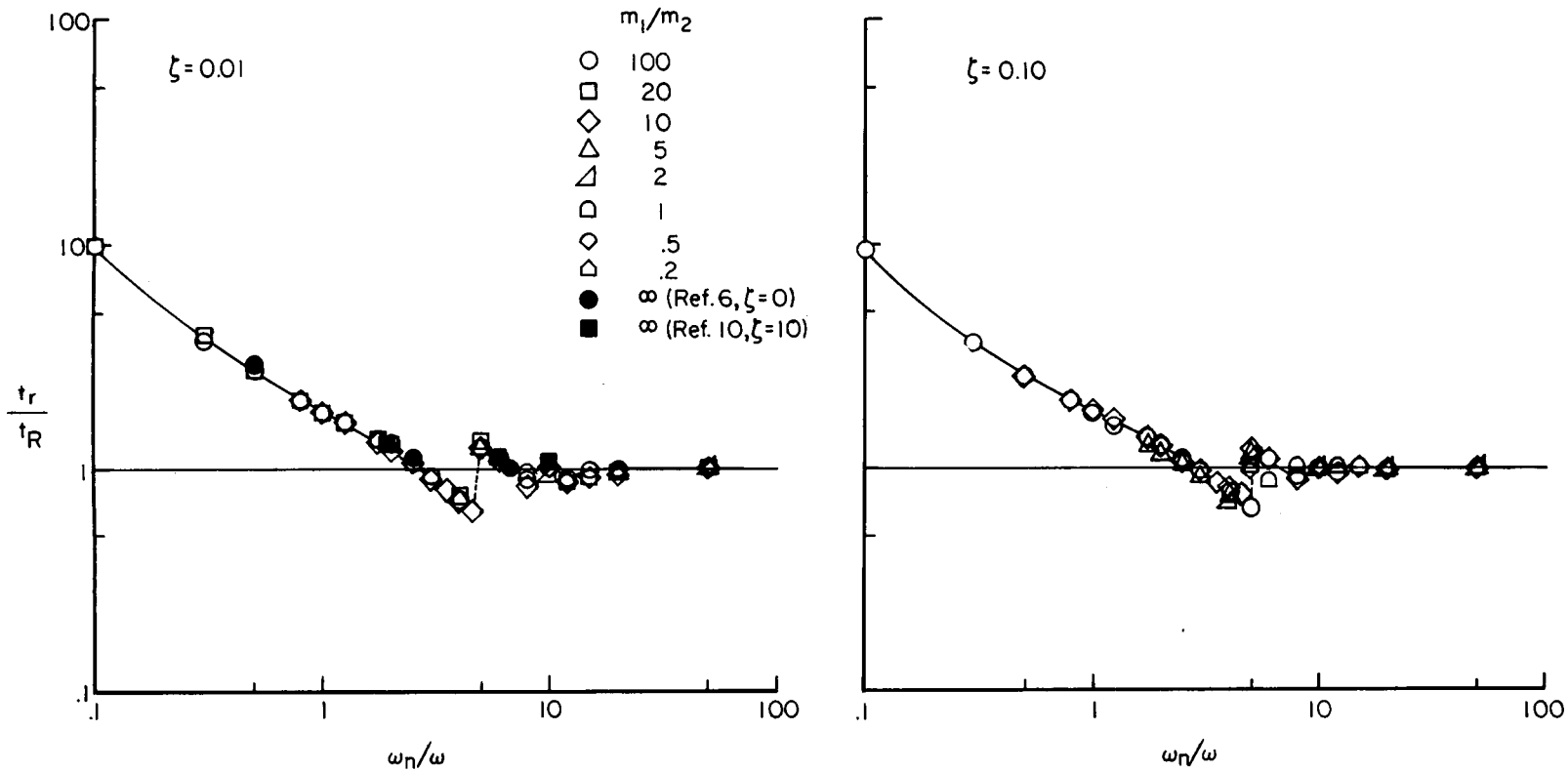

(a) Half-sine pulse.

Figure 12.- Rise time response of accelerometer assembly to various input pulses.

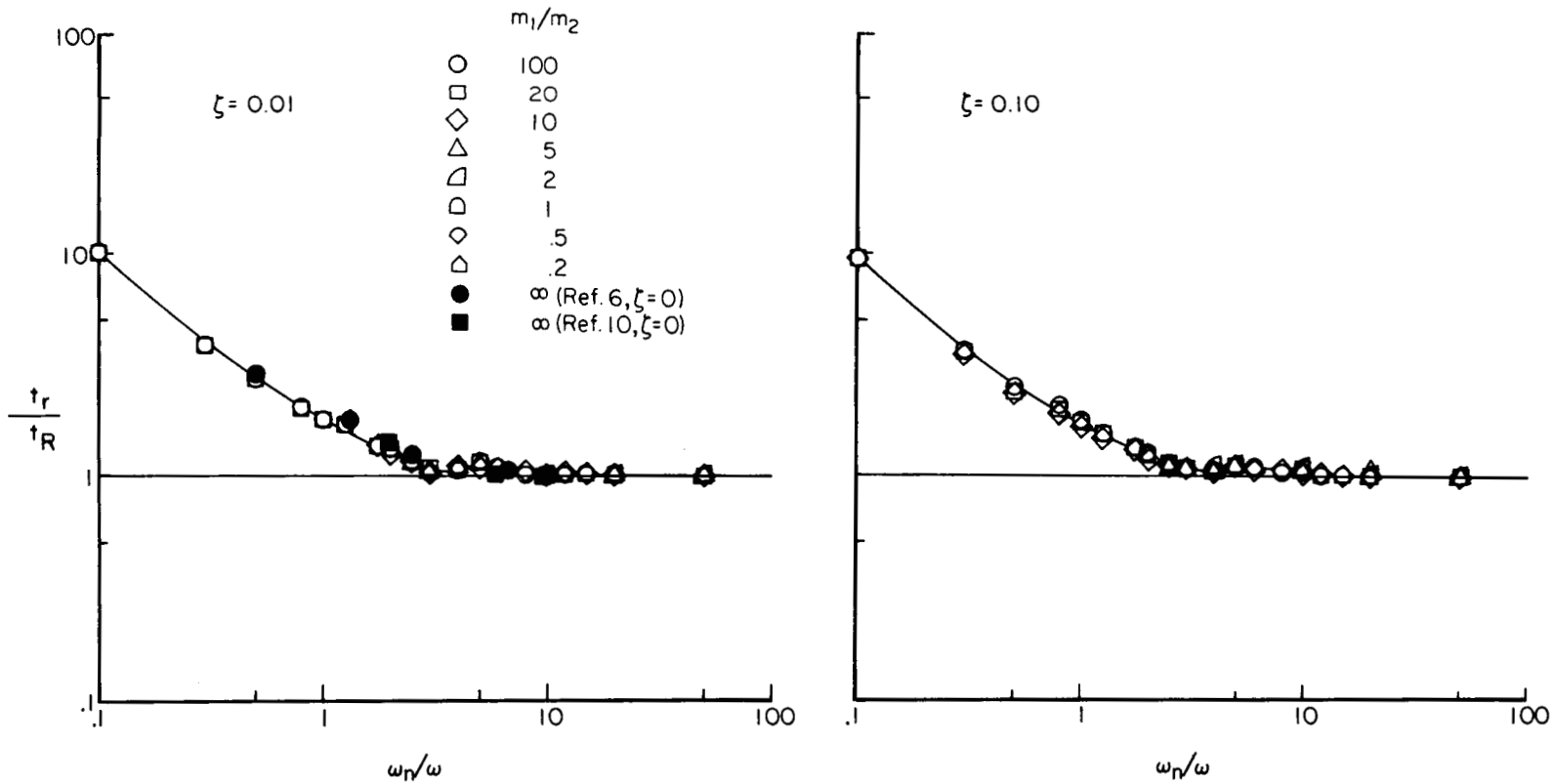

(b) Triangular pulse.

Figure 12.- Continued.

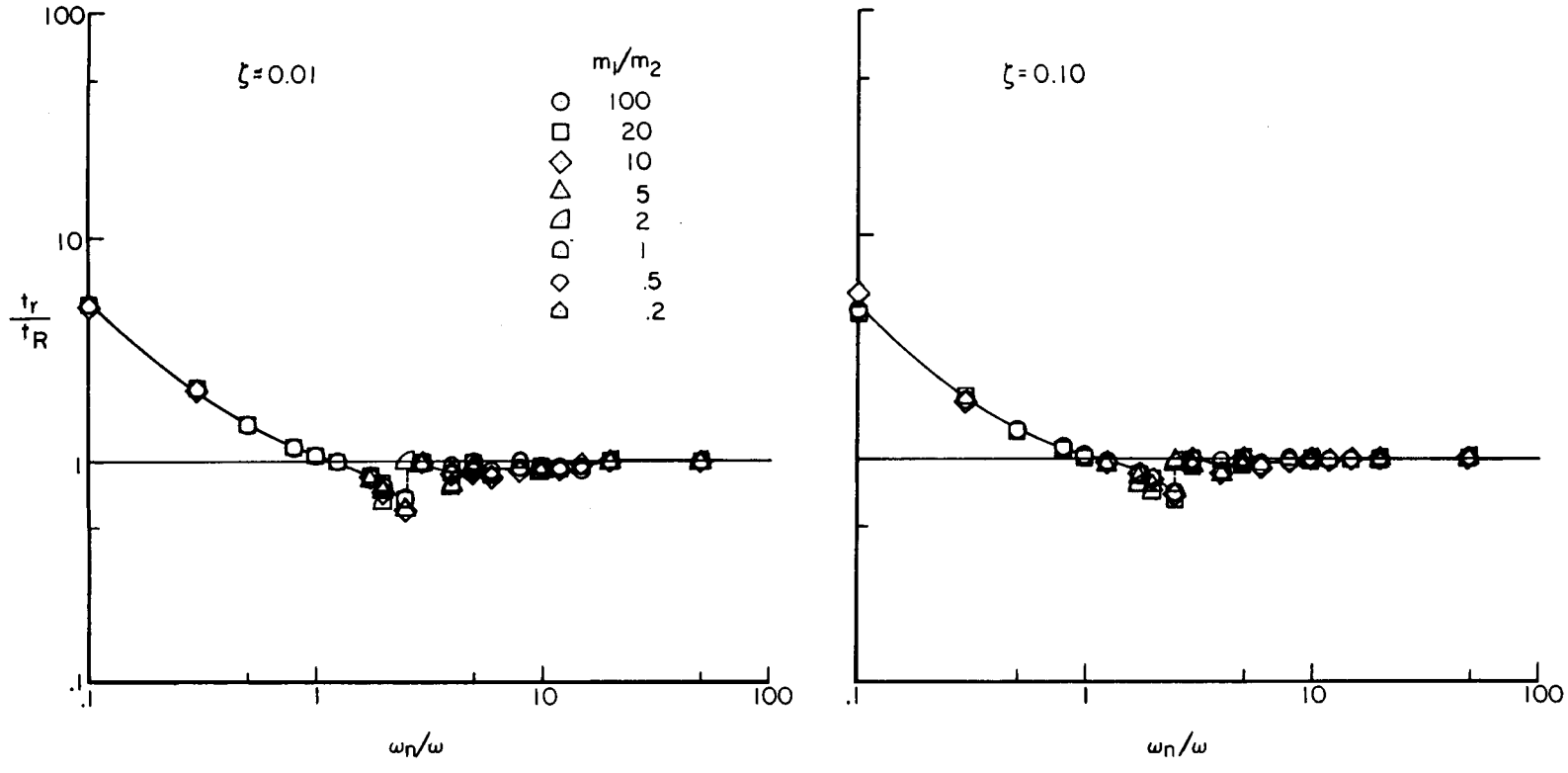

(c) Quarter-sine pulse.

Figure 12.- Concluded.

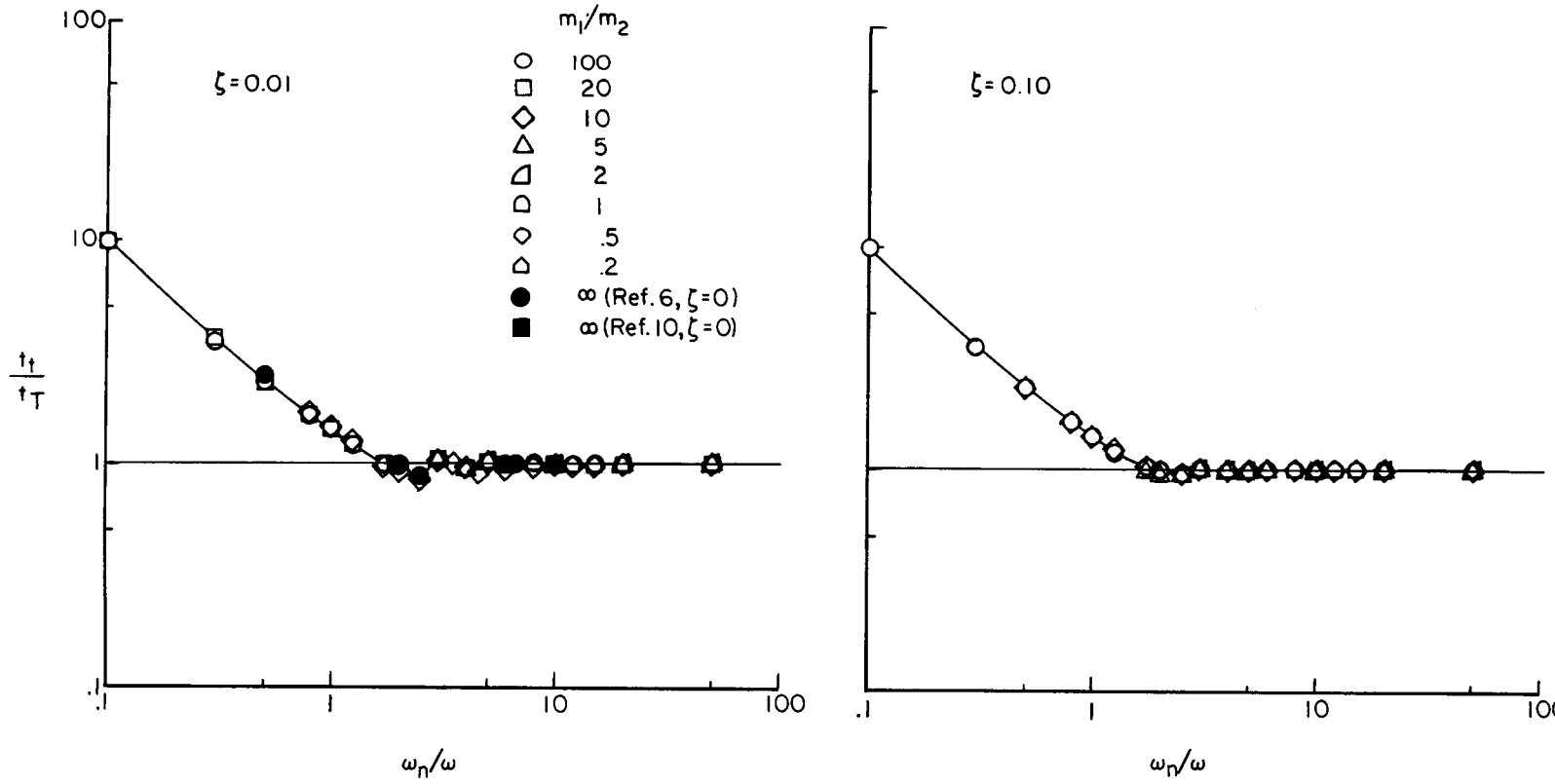

(a) Half-sine pulse.

Figure 13.- Total pulse time response of accelerometer assembly to various input pulses.

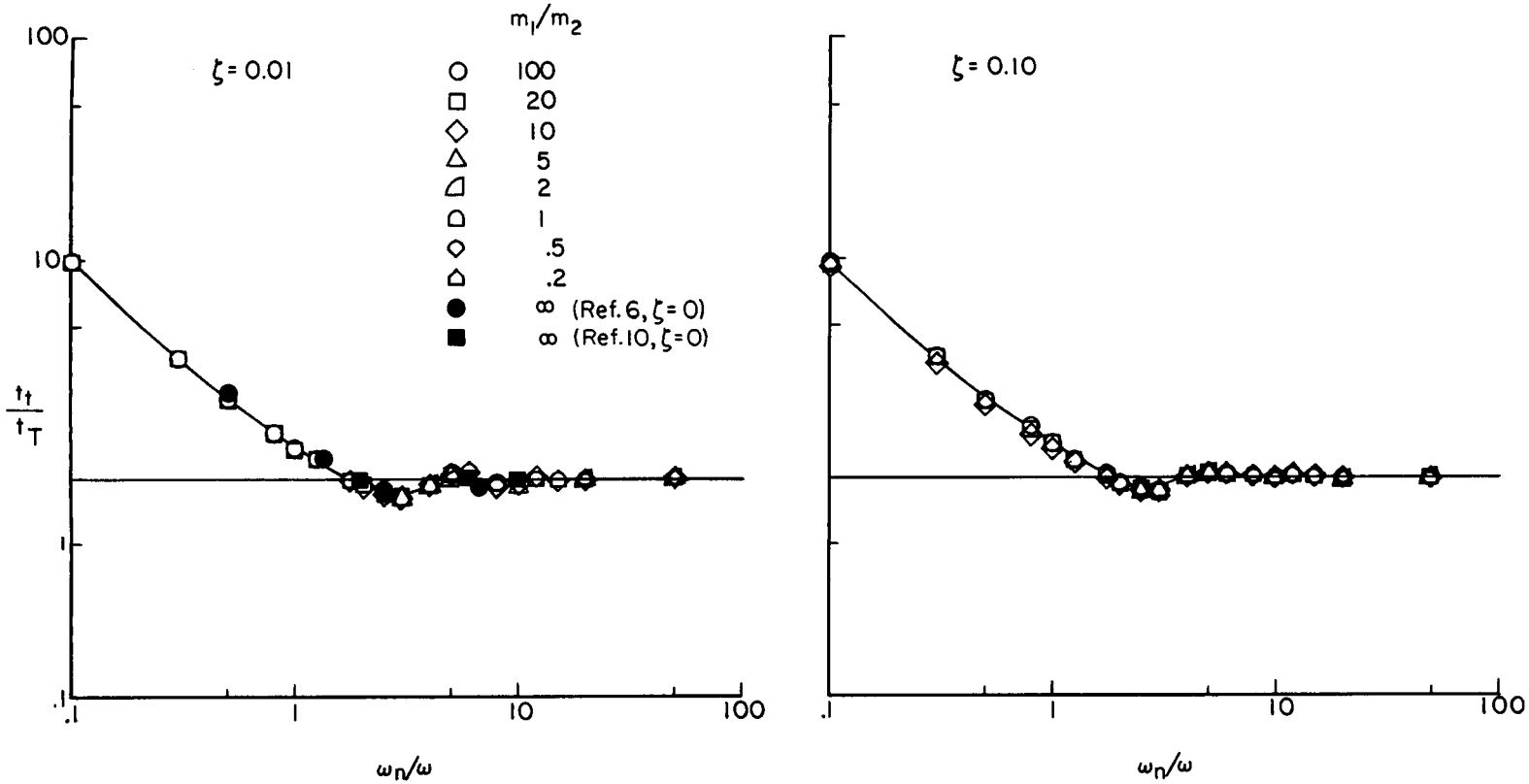

(b) Triangular pulse.

Figure 13.- Continued.

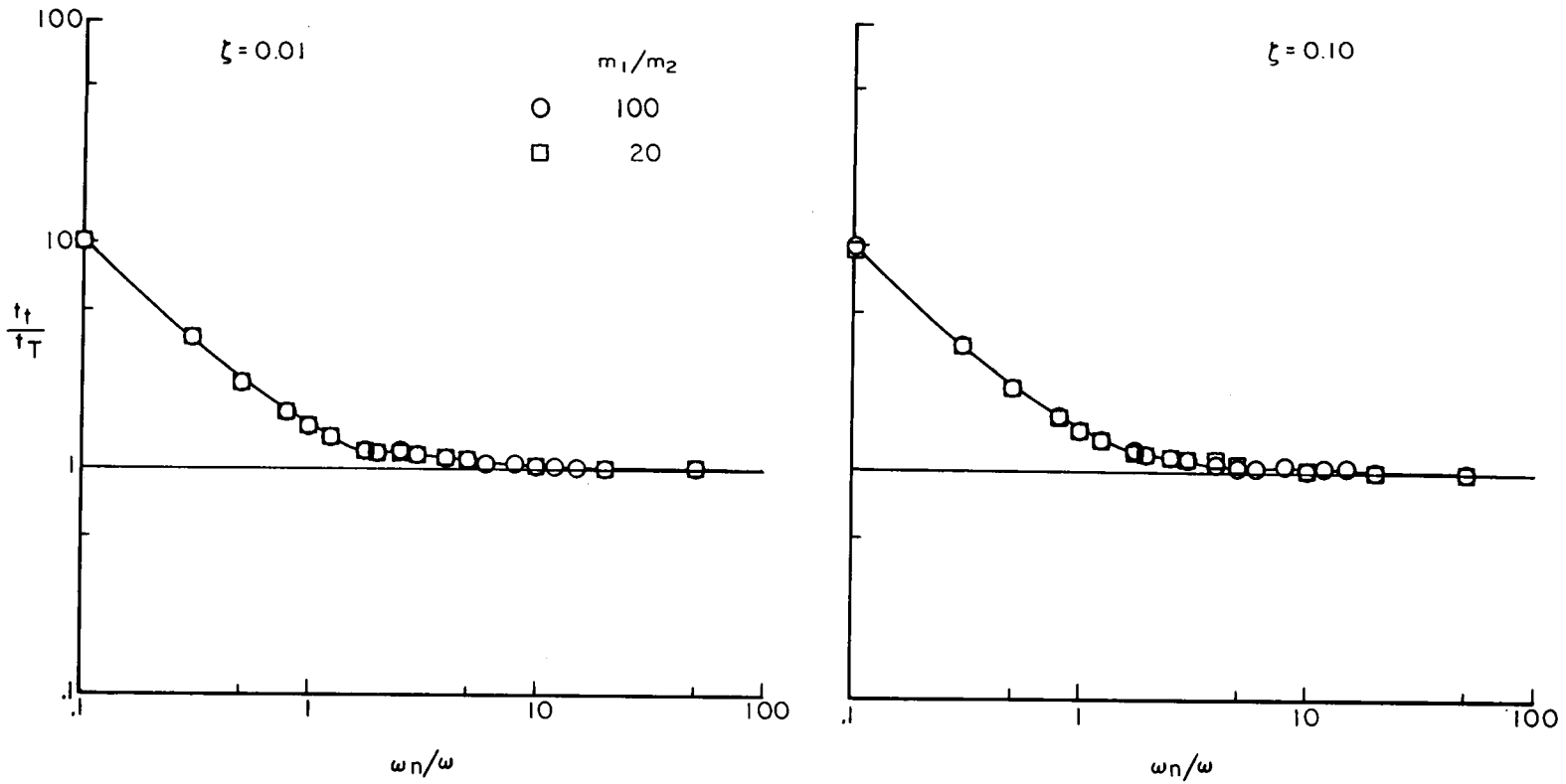

(c) Quarter-sine pulse.

Figure 13.- Continued.

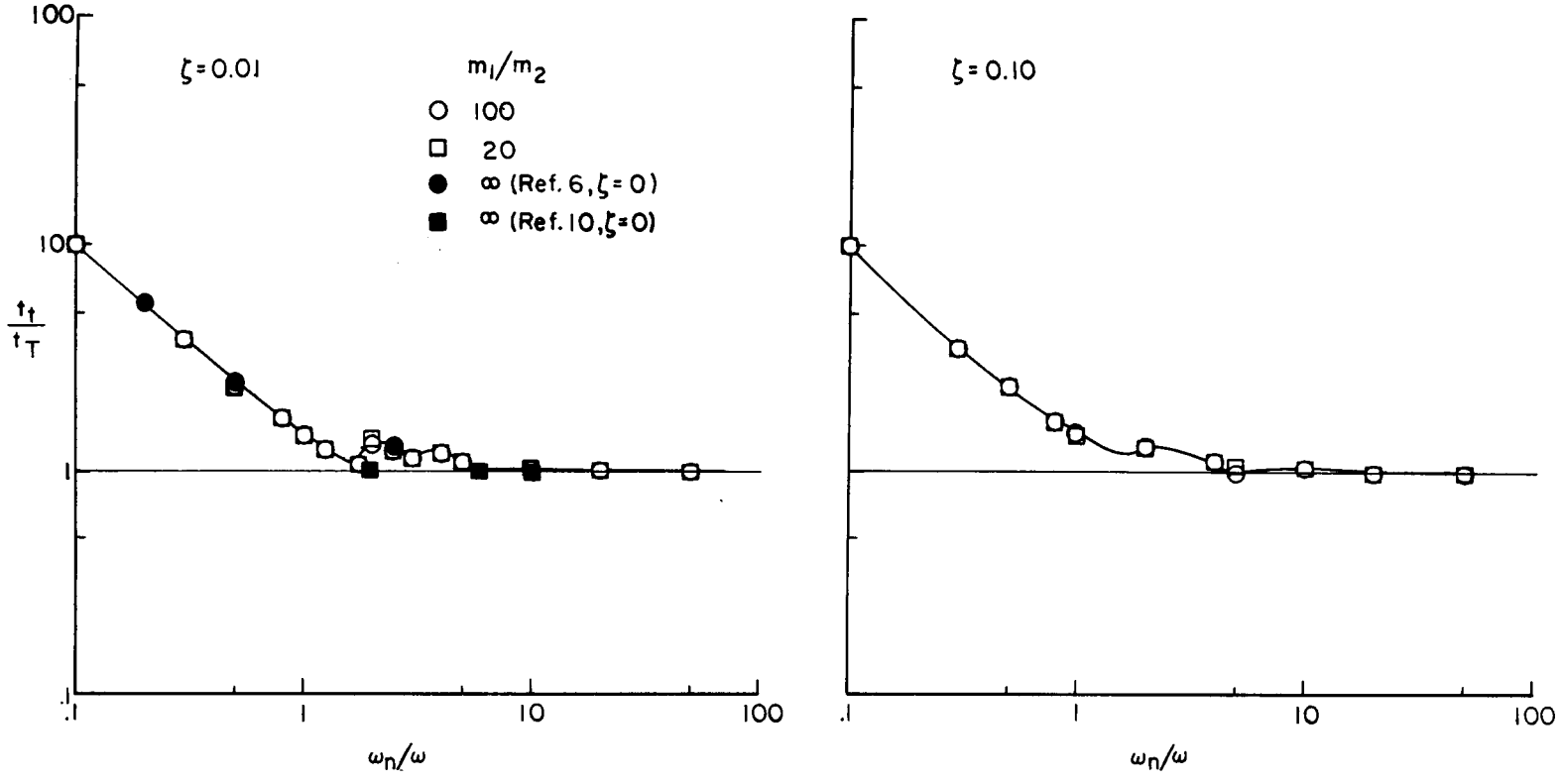

(d) Rectangular pulse.

Figure 13.- Concluded.

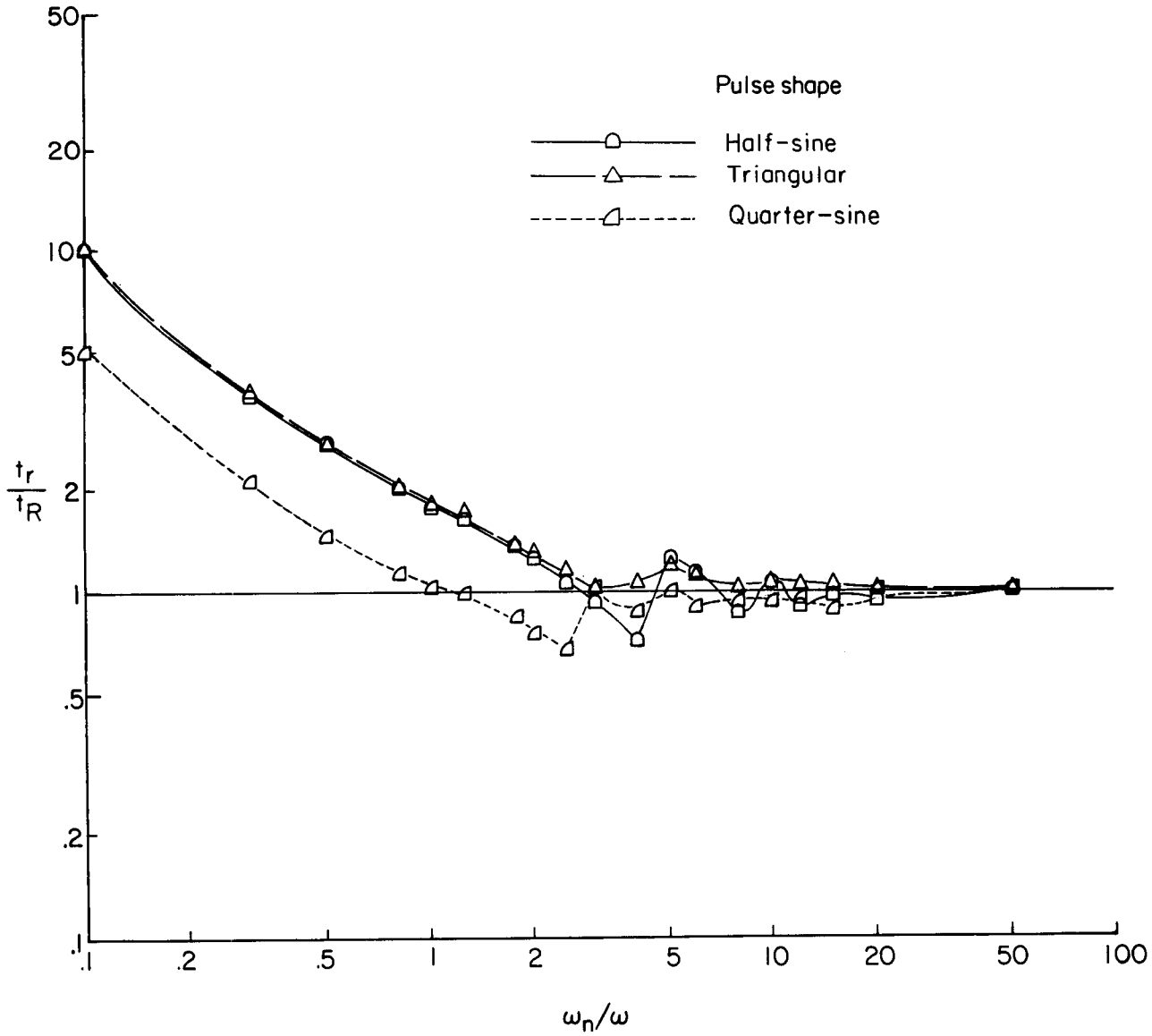

Figure 14.- Composite rise time response of accelerometer assembly to various pulse shapes. $m_1/m_2 = 100$; $\zeta = 0.01$.

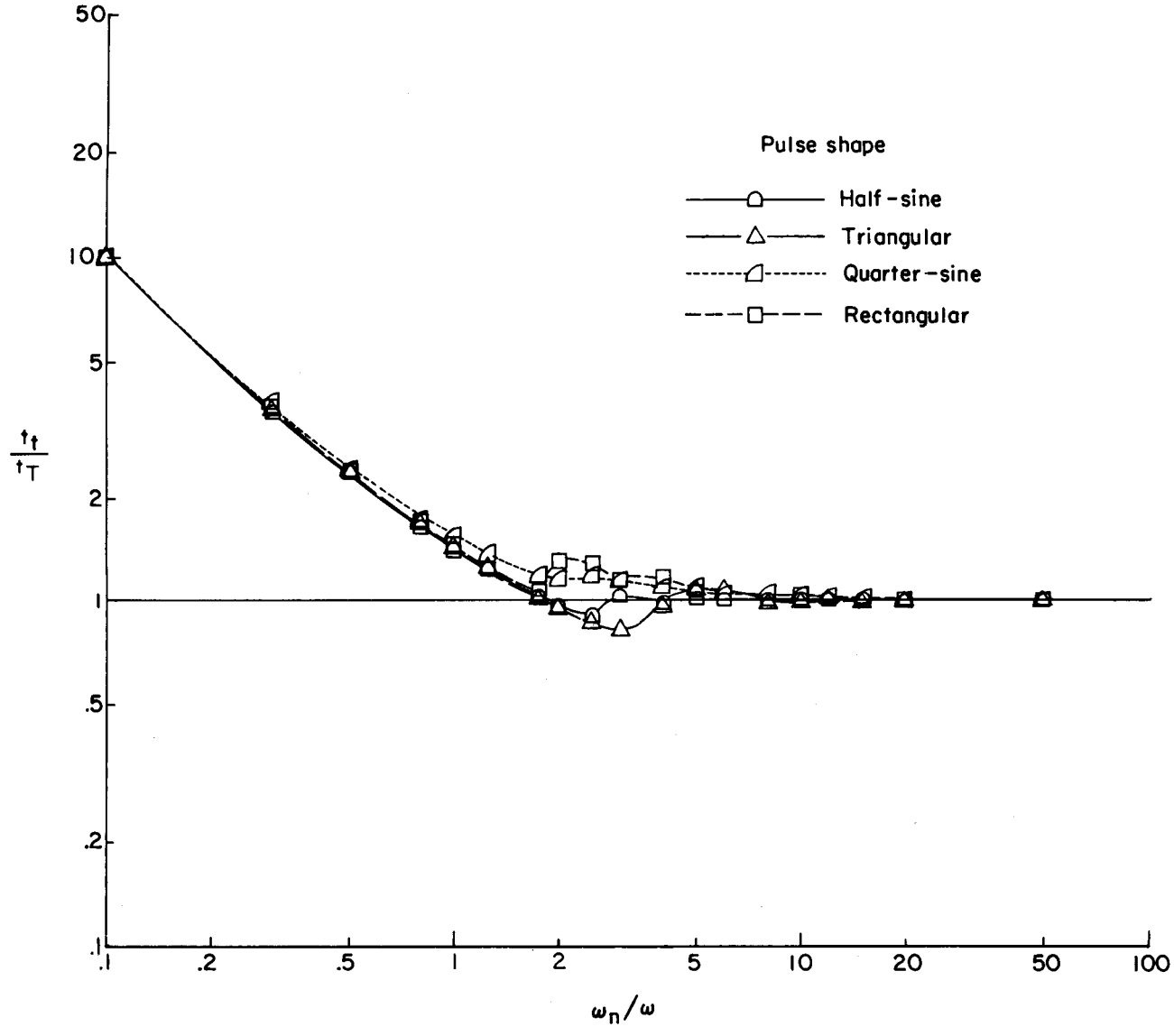

Figure 15.- Composite total pulse time response of accelerometer assembly to various pulse shapes. $m_1/m_2 = 100$; $\zeta = 0.01$.

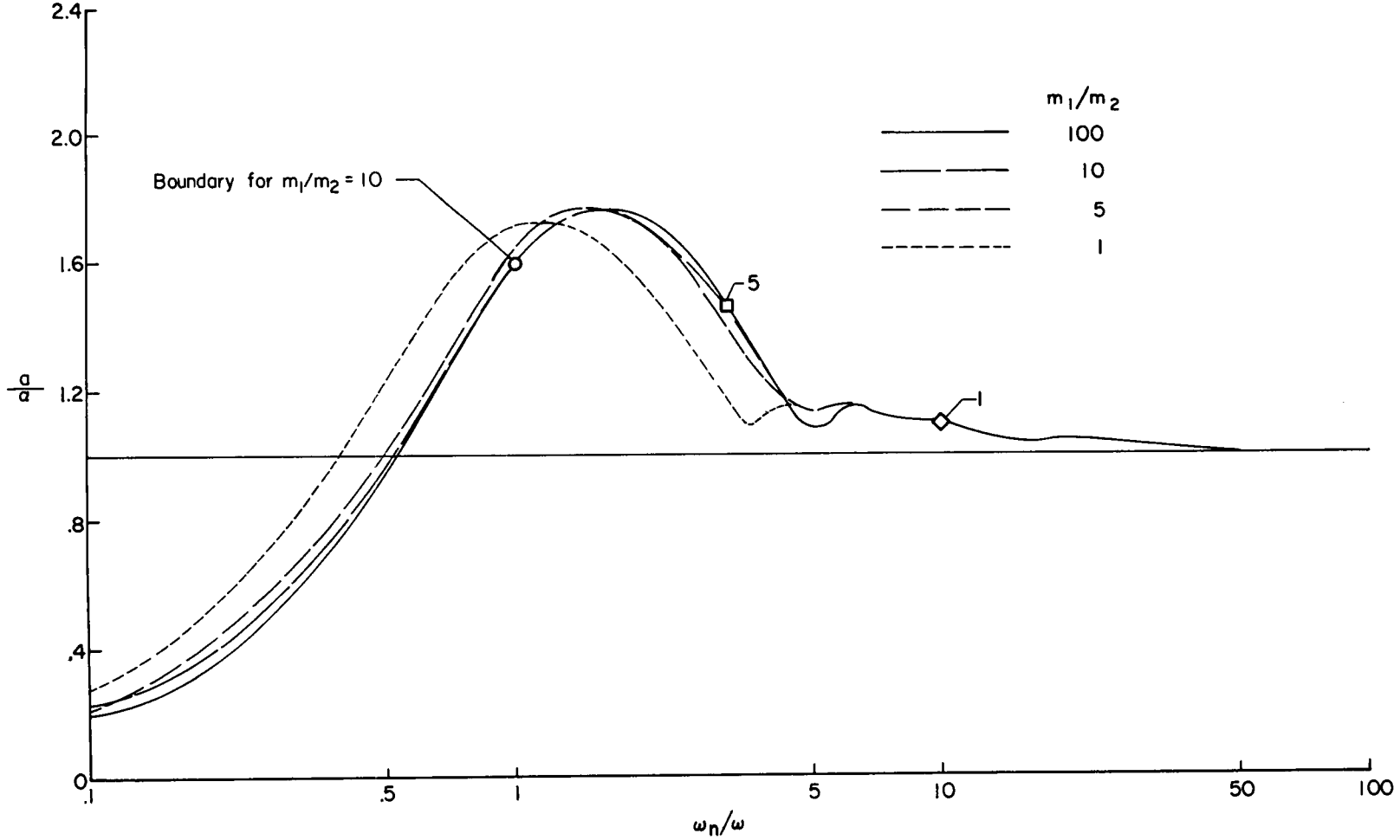

(a) Peak acceleration.

Figure 16.- Response of accelerometer assembly to half-sine input pulse illustrating significance of boundaries for application. $\zeta = 0.01$.

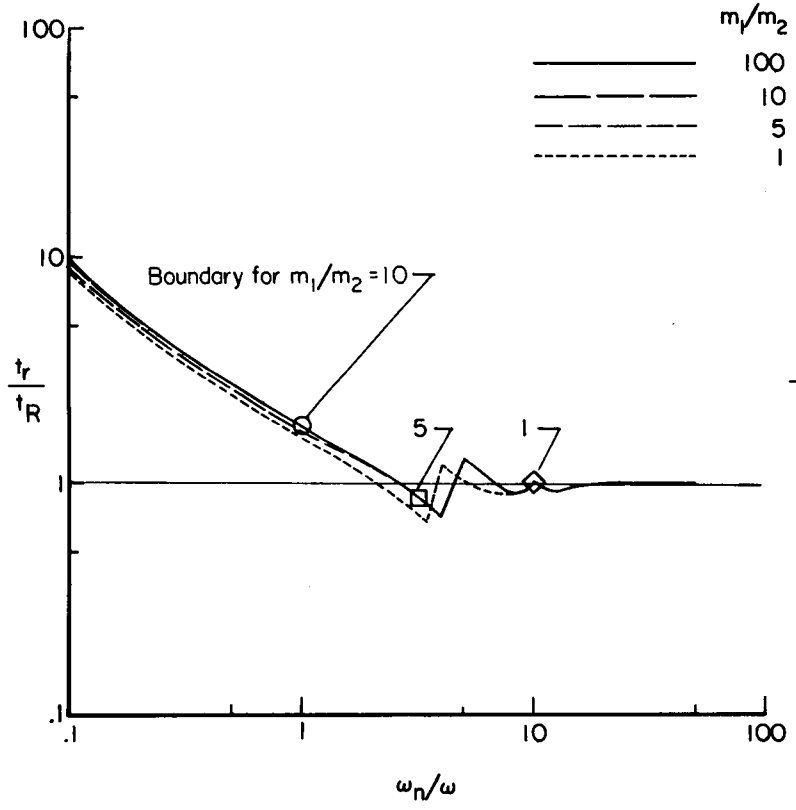

(b) Rise time.

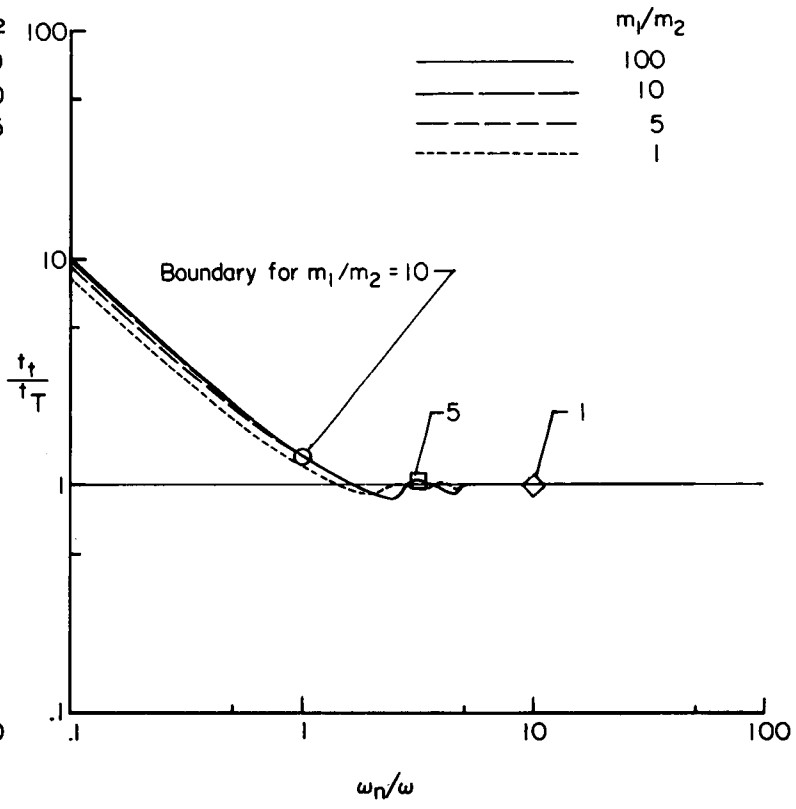

(c) Total pulse time.

Figure 16.- Concluded.

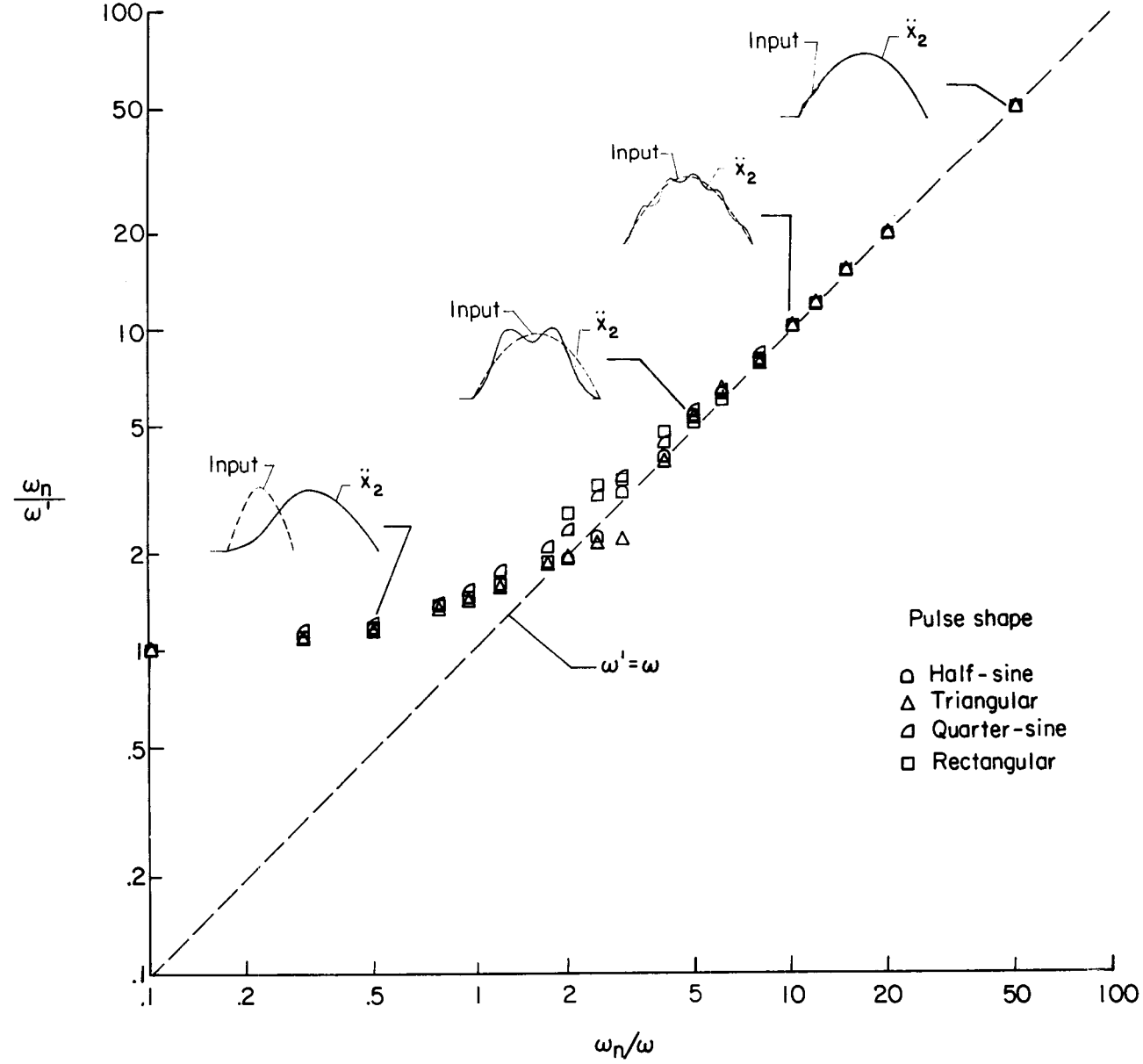

Figure 17.- Composite of data showing relationship between frequencies associated with the input pulse ω and the pulse of the accelerometer assembly response ω'. $m_1/m_2 = 100$; $\zeta = 0.01$.